



Statistical mechanics of plasticity: Elucidating anomalous size-effects and emergent fractional nonlocal continuum behavior

Pratik Khandagale ^a, Liping Liu ^{b,*}, Pradeep Sharma ^{c,*}

^a Department of Mechanical Engineering, University of Houston, Houston, TX 77204, USA

^b Department of Mathematics and Department of Mechanical and Aerospace Engineering, Rutgers University, NJ 08854, USA

^c Departments of Mechanical Engineering, Physics, and the Materials Science and Engineering Program, University of Houston, Houston, TX 77204, USA

ARTICLE INFO

Keywords:

Statistical mechanics
Plasticity
Long-range interactions
Size-effect
Fractional calculus

ABSTRACT

Extensive experiments over the decades unequivocally point to a pronounced scale-dependency of plastic deformation in metals. This observation is fairly general, and broadly speaking, strengthening against deformation is observed with the decrease in the size of a relevant geometrical feature of the material, e.g., the thickness of a thin film. The classical theory of plasticity is size-independent, and this has spurred extensive research into an appropriate continuum theory to elucidate the observed size effects. This pursuit has led to the emergence of strain gradient plasticity, along with its numerous variants, as the paradigm of choice. Recognizing the constrained shear of a thin metallic film as the model problem to understand the observed size-effect, all conventional (and reasonable candidate) theories of strain gradient plasticity predict a scaling of yield strength that inversely varies with the film thickness $\sim h^{-1}$. Experimental findings indicate a considerably diminished scaling, the magnitude of which can exhibit significant variation based on processing conditions or even the mode of deformation. As an example, the scaling exponent as low as -0.2 has been observed for as-deposited copper thin films. Two perspectives have been posited to explain this perplexing anomaly. Kuroda and Needleman (2019) argue that the conventional boundary conditions used in strain gradient plasticity theory are not meaningful for the canonical constrained thin film problem and propose a physically motivated alternative. Dahlberg and Ortiz (2019) contend that the intrinsic differential calculus structure of all strain gradient plasticity theories will invariably lead to the incorrect (or rather inadequate) explanation of the size-scaling. They propose a fractional strain gradient plasticity framework where the fractional derivative order is a material property that correlates with the scaling exponent. In this work, we present an alternative approach that complements the existing explanations. We create a statistical mechanics model for interacting microscopic units that deform and yield with the rules of *classical plasticity*, and plastic yielding is treated as a phase transition. We coarse-grain the model to precisely elucidate the microscopic interactions that can lead to the emergent size-effects observed experimentally. Specifically, we find that depending on the nature of the long-range microscopic interactions, the emergent coarse-grained theory can be of fractional differential type or alternatively a form of integral nonlocal model. Our theory, therefore, provides a partial (and microscopic) justification for the fractional derivative model and makes clear the precise microscopic interactions that must

* Corresponding authors.

E-mail addresses: liu.liping@rutgers.edu (L. Liu), psharma@central.uh.edu (P. Sharma).

<https://doi.org/10.1016/j.jmps.2024.105747>

Received 12 February 2024; Received in revised form 27 May 2024; Accepted 14 June 2024

Available online 8 July 2024

0022-5096/© 2024 Elsevier Ltd. All rights are reserved, including those for text and data mining, AI training, and similar technologies.

be operative for a continuum plasticity theory to be a valid phenomenological descriptor for capturing the correct size-scale dependency.

1. Introduction

The so-called *size-effect* in plasticity pertains to the augmentation of strength observed in a material undergoing inelastic deformation as a particular dimension or measure of its size diminishes. The central issue can be embodied by the following simple one-dimensional relation: $\sigma_y = \sigma_o[1 + (l/h)^\alpha]$ (Dahlberg and Ortiz, 2019). Here h is the relevant geometrical feature size, l and α are material properties that govern the scaling, while σ_y is the observed yield stress. Stipulating that deformation of a thin metallic film is an excellent paradigmatic problem from both a theoretical and experimental viewpoint; in that context, h may be identified with the film thickness. The classical theory of plasticity (Hill, 1998) is size-independent, and l is identically zero. Since the 1980s, there has been sustained and extensive effort to refine the theory of continuum plasticity in order to elucidate the size-effect, and this endeavor remains ongoing to the present day. In parallel, a wealth of experimental evidence has established the richness of scaling of plastic deformation in varied contexts e.g. twisting of wires (Fleck and Hutchinson, 2001; Dunstan et al., 2009; Liu et al., 2013), flexure in thin foils (Fleck and Hutchinson, 2001), micropillars in compression (Korte and Clegg, 2011), indentation hardness testing (Bushby and Dunstan, 2004) among many others cf. Xiang and Vlassak (2006), Fredriksson and Gudmundson (2005), Alizadeh et al. (2004). A general overview of size effects in micron-scale plasticity is provided in Greer and De Hosson (2011).

The conceptual foundation for enhancing the plasticity theory to encompass size-effects was derived from the concept of geometrically necessary dislocations and their correlation with nonhomogeneous deformation (Nye, 1953; Ashby, 1970; Gao and Huang, 2003). This led to the development of strain gradient plasticity theory and its numerous variations that currently abound in the literature (Mühlhaus and Alfantis, 1991; Fleck and Hutchinson, 2001; Gurtin and Anand, 2009; Fleck et al., 2015; Evans and Hutchinson, 2009; Idiart and Fleck, 2009a; Idiart et al., 2009; Niordson and Hutchinson, 2011; Dahlberg and Faleskog, 2013; Al-Rub and Voyiadjis, 2006; Evans and Hutchinson, 2009; Dahlberg and Ortiz, 2019; Kuroda and Needleman, 2019; Fleck et al., 1994; Hutchinson and Fleck, 1997). The prevailing strain gradient plasticity paradigm purports to modify the energy cost of deformation by adding strain gradient contributions, the strength of which is dictated by additional phenomenological material properties. This is in contrast to classical plasticity, which only contains energetic contributions from strain. The strain gradient plasticity theory as used currently (Mühlhaus and Alfantis, 1991; Fleck and Hutchinson, 2001; Han et al., 2005; Fleck et al., 2015; Gurtin and Anand, 2009; Gudmundson, 2004; Fleck and Willis, 2009a,b; Idiart and Fleck, 2009a; Niordson and Legartha, 2010; Dahlberg and Faleskog, 2013, 2014) are higher-order differential equations¹ and the additional material properties introduce a characteristic length scale that dictates the scaling (for instance, l in the equation of the topical paragraph).

The literature on the development and use of strain gradient plasticity theory is quite extensive, and we do not intend to provide a comprehensive review of the literature since that will unnecessarily distract from our central theme.² The key point to emphasize is that the exponent α in $\sigma_y = \sigma_o[1 + (l/h)^\alpha]$ is predicted to be one. Unfortunately, while strain gradient plasticity theories do predict a size-effect, the scaling is incorrect. Numerous experiments have shown that the exponent α can vary widely; for the very specific case of Copper, from 0.2 to 1 depending on the processing condition³ and deformation mode (Mu et al., 2014, 2016). The strong inverse size-dependency predicted by conventional strain gradient plasticity theories, as highlighted by Dahlberg and Ortiz (2019), is a consequence of the *differential calculus structure* of the governing equations. Perhaps due to that, the various extensions have been somewhat inadequate (at best) to redress this discrepancy. In summary, classical plasticity predicts no size-effect while strain gradient plasticity predicts an overtly strong size-effect and one that is rather restrictive and unable to capture the rich variation of scaling observed in experiments.⁴

We highlight two recent attempts to reconcile the discrepancy between the scaling predicted by current theories. The first is due to Dahlberg and Ortiz (2019), who contend that regardless of the flavor of the strain gradient plasticity theory being used, the inherent differential structure will lead to the inverse size-scaling with little latitude to capture the wide variation observed in experiments. They propose a fractional strain gradient plasticity theory⁵ where the order of the differential operator is no longer constrained to be an integer (as in conventional ordinary differential calculus). This derivative order, which can be a fraction, has

¹ The commonly strain gradient plasticity theories are fourth-order partial differential equations in terms of the displacement field in contrast to second order for classical plasticity.

² See Hutchinson and Fleck (1997), Voyiadjis and Song (2019), Evans and Hutchinson (2009), Gudmundson (2004), Fleck et al. (2015), Han et al. (2005) for review on strain gradient plasticity.

³ For example, in the case of constrained shear, the exponent was 0.2 for as-deposited state and 0.7 for the annealed state.

⁴ See the discussion in Dahlberg and Ortiz (2019) regarding modifications made by several authors (Evans and Hutchinson, 2009; Idiart et al., 2009; Idiart and Fleck, 2009b; Niordson and Hutchinson, 2011; Dahlberg and Faleskog, 2013; Al-Rub and Voyiadjis, 2006; Dahlberg and Boåsen, 2019).

⁵ There is increased recent interest in the broader physical sciences community to use fractional calculus to capture myriad non-classical features in physical phenomena such as in diffusion, viscoelasticity, material hereditaries, among others (Oates et al., 2021; Mashayekhi et al., 2018, 2019; Patnaik et al., 2020a,b; Hollkamp and Semperlotti, 2020; Ding et al., 2021; Li et al., 2019; Li and Ostoja-Starzewski, 2009; Deseri et al., 2016; Bologna et al., 2020; Ostoja-Starzewski, 2009, 2013; Lazopoulos, 2006).

the status of a material parameter and correlates with the scaling exponent α . With appropriate fitting, Dahlberg and Ortiz are able to match the experimentally observed weak size scaling.

Kuroda and Needleman take a very different approach (Kuroda and Needleman, 2019). Focusing primarily on the constrained shear problem of a thin metallic layer, they contend that there is nothing wrong with the conventional strain gradient plasticity theory but hypothesize that the failure is due to the assumed boundary condition of zero plastic strain at the interfaces of the thin film and the adjoining rigid materials. They propose to use a different boundary condition—prior to the initiation of plastic straining at the boundaries during a simple shear, the magnitude of plastic strain gradient at the layer boundary is constrained to be below a maximum threshold. The observed size scaling using this approach, with appropriate fitting, was able to match with the experimental results in Mu et al. (2014, 2016).

Further in-depth research is required to explore the connection of Kuroda and Needleman's interesting and illuminating approach (Kuroda and Needleman, 2019) to our work. The approach by Dahlberg and Ortiz is quite effective, but leaves open the question of the determination of the fractional derivative order and is used (at the moment) as a fitting parameter.⁶ This gives rise to the following questions: is there any microscopic way to justify fractional strain gradient plasticity or, further, actually determine the fractional derivative?

In this work, we propose a statistical mechanics model that, when coarse-grained, leads to an effective emergent theory of continuum plasticity. We purport to show that depending on the precise assumptions made at the microscale, classical plasticity or strain gradient plasticity theories emerge, but most interestingly, we are also able to justify a fractional strain gradient plasticity framework with a clear interpretation of the fractional derivative order. We remark that extensive work has been undertaken on statistical mechanics of dislocations (Berdichevsky, 2023; Soutyrine and Berdichevsky, 2018; Yefimov et al., 2004; El-Azab, 2000; Yefimov and Van der Giessen, 2005; Limkumnerd and Van der Giessen, 2008; Dimiduk et al., 2006; Sethna et al., 2017) and adjacent topics that are mathematically connected if not physically (Ahmadpoor et al., 2017; Zhu et al., 2022; Ahmadpoor et al., 2022; Grasinger et al., 2021; Grasinger and Sharma, 2024; Liu and Sharma, 2013).⁷ However, barring some simple results, the approach is rather difficult, with few analytical results at hand and certainly no clear pathway to justify a macroscopic theory that can explain the correct scaling observed experimentally. We, therefore, take an alternative approach, and our microscopic model posits that the material consists of several small regions (subunits) that reach different states of inelastic deformation obeying the rules of equilibrium statistical mechanics and *classical plasticity*.⁸ As with any statistical mechanics problems, we then characterize the energetic cost of deformation at the microscale (which includes the law of interaction between the subunits) and then perform suitable coarse-graining to find an effective free energy that governs the emergent or macroscale deformation behavior. The proposal to identify the microscale with smaller units of material that deform as per classical plasticity rather than contend with dislocations enormously simplifies the otherwise analytically intractable problem and permits us to obtain a wealth of insights.

The outline of the paper is as follows: in Section 2, we present an overview of the basic model premise and explain the kinematics and energetics at the microscale. Using the tools of equilibrium statistical mechanics, we obtain the macroscopic (coarse-grained) free energy of the body in Section 3. The microscale subunits can interact in different ways. As a first approximation, we assume that the interaction is negligible, and the analytical evaluation of such a model is presented in Section 4. In Section 5, we derive the details of the model when interactions⁹ are incorporated and elucidate the underpinnings of the size-effect. Aside from concluding in Section 6, we highlight several details in the appendices.

2. Central premise and energetics of uniform states

The central premise of the model is depicted in Fig. 1. We consider a plastically deforming body¹⁰ under homogeneous applied stress $\bar{\sigma}$. The body is divided into smaller elasto-plastic micro-regions, where each micro-region is equivalent to a single element in the lattice. Elastic and plastic strain in every single element is assumed to be fluctuating and homogeneous within the element. The microscopic energy of each element is composed of linear elastic energy and activation energy for plastic strain modeled using an energy barrier. We treat the body as an ensemble of all the elements in the statistical mechanics framework. Without the loss of generality and detracting from the central goal of our paper, we adopt a minimum model of plasticity (*ideal plasticity*). A remedy to introduce strain-hardening and strain-softening responses using microscopic mechanisms is discussed in Appendix C. Each sub-unit can interact with others through some interaction law. Physically, this situation is similar to interacting dislocations¹¹ or closer to our schematic model, the interaction of two inclusions with an inelastic eigenstrain.¹² The interaction among the elements is assumed to be pairwise, isotropic, and repulsive, but a detailed discussion regarding its subtleties is deferred to Section 5.2.

⁶ This is not a criticism. All phenomenological theories use fitting parameters, as do we in the current work. Our emphasis in this manuscript is on microscopic and physical justification.

⁷ See an interesting application and examples of statistical mechanics in the context of grain boundaries (Chen and Kulkarni, 2015, 2013, 2017).

⁸ Indeed, the highlight of our work is that even though at the microscale, deformation is assumed to obey classical size-independent plasticity, fractional strain gradient plasticity can emerge as an effective macroscopic descriptor.

⁹ The many-body interactions play a critical role in many scientific fields of interest, such as elasticity (Eringen, 1972; Kröner, 1967), polymer networks (Khandagale et al., 2023), dielectric polymers (Khandagale et al., 2024), ionic solids (Marshall and Dayal, 2014), quantum theory (Yukawa, 1950; Bruus and Flensberg, 2004), and more (Jha et al., 2023; Abkevich et al., 1995; Di Paola and Zingales, 2008; French et al., 2010; Campa et al., 2009).

¹⁰ See Rohrer et al. (2023) for the evolution of the microstructure of polycrystalline metals through the mechanism of grain boundary migration.

¹¹ Recall that two isolated dislocations in an infinite elastic medium interact as $\ln r$.

¹² The situation of two regions in a body undergoing slightly different inelastic deformation is very close to the interaction of two Eshelby-type inclusions. Recall that two inclusions with an inelastic eigenstrain exhibit an asymptotic interaction of $1/r^2$.

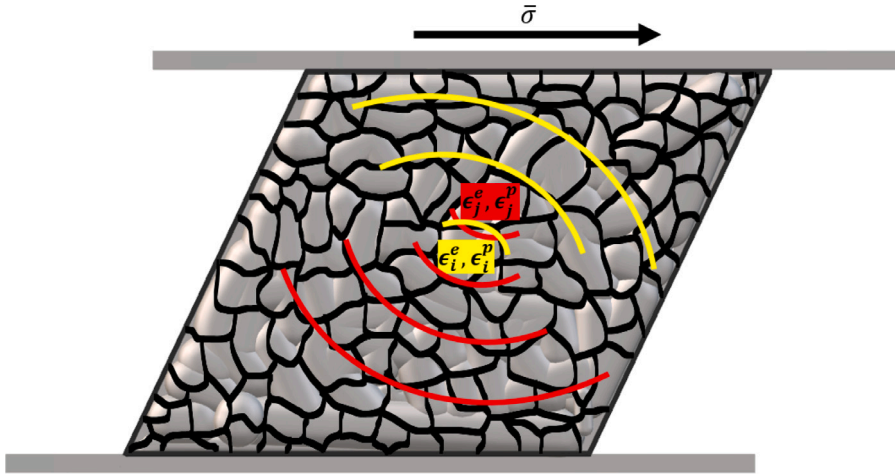


Fig. 1. Schematic of interactions among microscopic plastic regions in a sample undergoing plastic shear deformation between two rigid plates.

We first consider the microscopic kinematics and energetics of a single element in the body. As illustrated in Fig. 1, consider a representative element in d -dimensional space, say, $[0, \xi_c]^d$ with $\xi_c > 0$ being the relevant lengthscale. For simplicity, we employ geometrically linear kinematics in the sense that the total shear strain of the element is the sum of elastic strain and plastic strain:

$$\epsilon = \epsilon^e + \epsilon^p.$$

Under the application of shear stress $\bar{\sigma}$, we propose that the total energy (or Hamiltonian) of an element as a function of elastic–plastic strains (ϵ^e, ϵ^p) can be written as

$$\begin{aligned} \hat{H}(\epsilon^e, \epsilon^p; \bar{\sigma}) &= \hat{H}_0(\epsilon^e, \epsilon^p; \bar{\sigma}) + \hat{H}^{\text{dsp}}(\epsilon^p), \\ \hat{H}_0(\epsilon^e, \epsilon^p; \bar{\sigma}) &= v_c \left[\frac{1}{2} G (\epsilon^e)^2 - \bar{\sigma} \epsilon \right], \quad \hat{H}^{\text{dsp}}(\epsilon^p) = \gamma (\epsilon^p) \xi_c, \end{aligned} \tag{2.1}$$

where $G > 0$ is the shear modulus, $v_c = (\xi_c)^d$ is the volume of the element, and $\gamma(\epsilon^p) > 0$ is the activation force of plastic strain. Physically, we recognize $\hat{H}_0(\epsilon^e, \epsilon^p; \bar{\sigma})$ as the sum of the elastic energy ($\frac{1}{2} G (\epsilon^e)^2$) and potential energy ($-\bar{\sigma} \epsilon$) associated with applied stress $\bar{\sigma}$, and $\hat{H}^{\text{dsp}}(\epsilon^p)$ as the energy dissipation associated with plastic strain.

The admissible plastic strain is *a priori* assumed to be discrete with *quanta* of plastic strain:

$$\epsilon^p = k \epsilon_*^p \quad (k \in \mathbb{Z}). \tag{2.2}$$

With inspiration from the dislocation theory of crystalline solids, we can relate a quantum of plastic strain with the magnitude of Burgers vector b : $\epsilon_*^p \sim \frac{b^2}{\xi_c^2}$. Here, we aim to develop a generic statistical model for plasticity originating from microscopic mechanisms.

Therefore, we will not specify the value of quanta of plastic strain ϵ_*^p , though $\frac{b^2}{\xi_c^2}$ is a reasonable order-of-magnitude estimate.

Based on symmetry and stability, we require that the activation force (or activation energy per unit length) $\gamma = \gamma(\epsilon^p)$ satisfies the following conditions:

- (i) $\gamma(0) = 0$ and $\gamma(\epsilon^p) > 0$ if $\epsilon^p \neq 0$;
- (ii) $\gamma(-\epsilon^p) = \gamma(\epsilon^p)$.

Again, inspired by dislocation theory, the activation force $\gamma(\epsilon_*^p)$ for one quantum of plastic strain could be identified as the Peierls-Nabarro type energy barrier. Below, we list a few possible choices of activation energy for plastic strains.

1. For a minimum model, we postulate that ($\hat{\epsilon}^p = \frac{\epsilon^p}{\epsilon_*^p}$)

$$\gamma(\epsilon^p) = \gamma_0 Q\left(\frac{\epsilon^p}{\epsilon_*^p}\right), \quad Q(x) = |x| + c_1 |x|^2, \tag{2.3}$$

where $\gamma_0 \geq 0$ and $c_1 \in \mathbb{R}$ are some empirical coefficients.

2. More generally, we may assume that

$$\gamma(\epsilon^p) = \gamma_0 A\left(\frac{\epsilon^p}{\epsilon_*^p}\right), \quad A(x) = |x| + \sum_{n=1}^{\infty} c_n |x|^{n+1} = |x| + c_1 |x|^2 + \dots \tag{2.4}$$

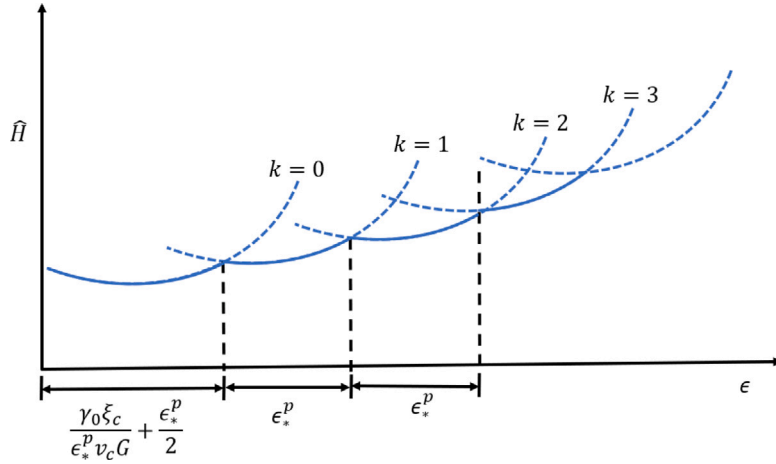


Fig. 2. Total energy of a single element (\hat{H} ; shown in solid line) plotted for different strain (ϵ) values. Different parabolas correspond to different $k \in \mathbb{Z}$.

3. To accommodate various physical origins of plastic strains at different stages of deformation, we may assume a piecewise linear activation energy of form:

$$\gamma(\epsilon^p) = \gamma_0 S\left(\frac{\epsilon^p}{\epsilon_*^p}\right), \quad S(x) = \begin{cases} x & \text{if } 0 < x \leq \epsilon_1^p / \epsilon_*^p, \\ c_1(x - \epsilon_1^p / \epsilon_*^p) + \epsilon_1^p / \epsilon_*^p & \text{if } \epsilon_1^p / \epsilon_*^p < x \leq \epsilon_2^p / \epsilon_*^p, \\ \vdots & \vdots \end{cases} \quad (2.5)$$

Presumably, various forms of activation energy (2.3)–(2.5) can be used to model plastic behaviors from different mechanisms, including movements of dislocations, nucleations of new dislocations, nucleations of voids and interstitial sites, etc. Subsequently, we choose a particular form of activation energy at the phenomenological level without attempting to associate an activation energy form with a particular mechanism. Under the application of the external stress $\bar{\sigma}$ and neglecting the influence of thermal fluctuations, we claim the equilibrium state of the element is governed by the minimization problem:

$$\min\{\hat{H}(\epsilon^e, \epsilon^p; \bar{\sigma}) : \epsilon \in \mathbb{R}, \epsilon^p \in \epsilon_*^p \mathbb{Z}\}. \quad (2.6)$$

Suppose that the activation energy $\gamma = \gamma(\epsilon^p)$ is given by (2.3) with $c_1 \equiv 0$. The solid line in Fig. 2 shows the total energy \hat{H} plotted for different total strain $\epsilon = \epsilon^e + \epsilon^p$, where each parabola corresponds to different $k \in \mathbb{Z}$. Following (2.6), the first order necessary condition for the minimum energy, $\frac{\partial \hat{H}}{\partial \epsilon} = 0$ gives us the applied stress ($\bar{\sigma}$) in terms of strain (ϵ) as a discontinuous, piecewise linear function given by

$$\bar{\sigma} = \begin{cases} G\epsilon & \text{if } 0 < \epsilon < \frac{\sigma_Y}{G} + \frac{1}{2}\epsilon_*^p \\ G(\epsilon - k\epsilon_*^p) & \text{if } \frac{\sigma_Y}{G} + \frac{2k-1}{2}\epsilon_*^p < \epsilon < \frac{\sigma_Y}{G} + \frac{2k+1}{2}\epsilon_*^p \quad k = 1, 2, 3, \dots, \end{cases} \quad (2.7)$$

which is illustrated in Fig. 3. The stress

$$\sigma_Y = \frac{\gamma_0 \xi_c}{v_c \epsilon_*^p} \quad (2.8)$$

may be identified as the critical stress for driving the dislocation over the energy barrier or the yield stress at the absence of (thermal or structural) fluctuations.

3. Free energy of a lattice model

In this section, we present the treatment of statistical mechanics to obtain the coarse-grained free energy of the plastically deforming body. Consider a macroscopic sample of size L in \mathbb{R}^d . Upon subdividing the sample into $N = (L/\xi_c)^d$ elements, we are interested in finding the macroscopic properties of the sample by the principles of statistical physics. For each of the elements, the states (or DOFs) of each element are described by two variables, i.e., the elastic and plastic strains $(\epsilon_i^e, \epsilon_i^p)$, with the discrete admissible spaces identified as

$$\mathbb{S} = \mathbb{S}^e \times \mathbb{S}^p, \quad \mathbb{S}^e := \epsilon_0 \mathbb{Z}, \quad \mathbb{S}^p := \epsilon_*^p \mathbb{Z}. \quad (3.1)$$

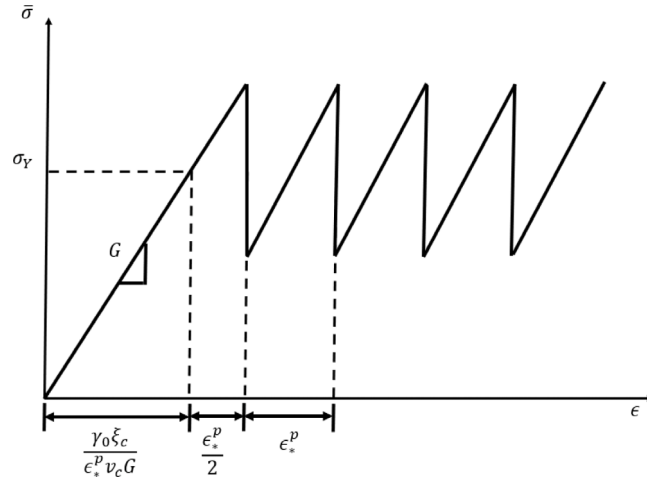


Fig. 3. Microscopic elasto-plastic behavior of a single element.

Here, ϵ_0 ($0 < \epsilon_0 \ll \epsilon_*^p$) is a positive constant for counting elastic-strain whose precise value is of no physical consequence, and \mathbb{S} is the collection of single-site states for a representative element. The configurational space for microstates of the entire sample with N elements is given by

$$\Omega = \mathbb{S}^N. \tag{3.2}$$

In other words, a microstate of the system $s \in \Omega$ contains N pairs of $(\epsilon_i^e, \epsilon_i^p) \in \mathbb{S}$ with i being the label for each element. Suppose that the probability that the system is found at the s -microstate is given by $p(s)$. Then, the averages or expectations of elastic and plastic strain at the i th site can be written as

$$\langle \bar{\epsilon}_i^e, \bar{\epsilon}_i^p \rangle = (\langle \epsilon_i^e(s) \rangle, \langle \epsilon_i^p(s) \rangle) = \left(\sum_{s \in \Omega} \epsilon_i^e(s) p(s), \sum_{s \in \Omega} \epsilon_i^p(s) p(s) \right),$$

and the macroscopic elastic and plastic strain are defined as the averages:

$$\langle \bar{\epsilon}^e, \bar{\epsilon}^p \rangle = \frac{1}{N} \sum_{i=1}^N (\langle \epsilon_i^e(s) \rangle, \langle \epsilon_i^p(s) \rangle). \tag{3.3}$$

From discussions in Section 2, the Hamiltonian for the system is postulated as

$$\begin{aligned} H(s; \bar{\sigma}) &= H_0(s; \bar{\sigma}) + H^{\text{int}}(s), \\ H_0(s; \bar{\sigma}) &= \sum_{i=1}^N \hat{H}(\epsilon_i^e, \epsilon_i^p; \bar{\sigma}) = \sum_{i=1}^N \left\{ v_c \left[\frac{1}{2} G (\epsilon_i^e)^2 - \bar{\sigma} \epsilon_i \right] + \gamma (\epsilon_i^p) \xi_c \right\}, \end{aligned} \tag{3.4}$$

where $\bar{\sigma}$ is the applied external shear stress, and $H^{\text{int}}(s)$ represents the interaction energy between elements whose precise form will be specified later.

To pass from the microscopic model described by the Hamiltonian (3.4) to a macroscopic coarse-grained model, we will employ the approach of statistical physics. In classical thermal physics, the critical concept of (absolute) temperature reflects the collective energy states and fluctuations within the system, whereas entropy measures the number of accessible microstates of the system. In thermal equilibrium, the probability distribution over all admissible microstates of the system is dictated by the Second Law, which can then be used to determine all macroscopic properties (or thermodynamic relations) of the system. To apply this approach to a plastically deformed body, we postulate the following.

1. The stochasticity or fluctuations are macroscopically homogeneous within the system (an elastoplastic body) and can still be characterized by a single positive parameter called *temperature* T . As a microscopic statistical model, the temperature here characterizes stochasticity contributed by thermal agitations and other sources, including but not limited to structural defects and pre-existing heterogeneities in the materials. Therefore, T should be understood as some kind of empirical parameter instead of the actual thermal temperature that originates from the vibration of atoms.¹³ The physically relevant parameter is the energy scale $k_B T$ (k_B is the Boltzmann constant). Similar ideas have been used in the literature for studying glassy polymers, granular mechanics, and amorphous materials.

¹³ Although we interpret temperature T here as an empirical parameter, we have scaled the lengthscale of unit plastic microregion (ξ_c) such that the value of temperature T in our analysis stays in the physical range of absolute temperature for the material under investigation.

2. In quasi-static processes of deformation by applied stress $\bar{\sigma}$, the sample may exchange energy with the environment and stay in instantaneous equilibrium at a constant temperature T , and hence follows the Maxwell–Boltzmann distribution.

Based on these postulates, we consider a canonical ensemble of the system at a constant temperature T and claim that the probability distribution $p(s)$ over all admissible microstates of the system is given by the Maxwell–Boltzmann distribution: ($\beta = 1/k_B T$)

$$p(s) = \frac{e^{-\beta H(s; \bar{\sigma})}}{Z} \quad (\forall s \in \Omega), \quad (3.5)$$

where

$$Z(\beta, N, \bar{\sigma}) = \sum_{s \in \Omega} e^{-\beta H(s; \bar{\sigma})} = \sum_{s \in \Omega} e^{-\beta H^{\text{int}}(s)} e^{-\beta \sum_{i=1}^N \left\{ v_c \left[\frac{1}{2} G(\epsilon_i^e)^2 - \bar{\sigma} \epsilon_i \right] + \gamma(\epsilon_i^p) \xi_c \right\}} \quad (3.6)$$

is the partition function. Moreover, the free energy of the system is given by

$$F(\beta, N, \bar{\sigma}) = -k_B T \log Z(\beta, N, \bar{\sigma}). \quad (3.7)$$

Direct differentiation implies the familiar thermodynamic relations:

$$-\frac{\partial F(\beta, N, \bar{\sigma})}{\partial \bar{\sigma}} = \sum_{s \in \Omega} \left[\frac{e^{-\beta H(s; \bar{\sigma})}}{Z} v_c \sum_{i=1}^N \epsilon_i(s) \right] = \frac{V}{N} \sum_{i=1}^N \langle \epsilon_i \rangle = V \bar{\epsilon}. \quad (3.8)$$

Taking another derivative of the above equation, we obtain

$$\begin{aligned} \frac{V}{G^{\text{eff}}} &:= -\frac{\partial^2 F}{\partial \bar{\sigma}^2} = \beta \sum_{s \in \Omega} \left\{ \frac{e^{-\beta H(s; \bar{\sigma})}}{Z} \left[v_c \sum_{i=1}^N \epsilon_i(s) \right]^2 \right\} - \beta \sum_{s \in \Omega} \left\{ \frac{e^{-\beta H(s; \bar{\sigma})}}{Z} v_c \sum_{i=1}^N \epsilon_i(s) \right\}^2 \\ &= \frac{\beta V^2}{N^2} \sum_{i=1}^N [\langle \epsilon_i^2 \rangle - \langle \epsilon_i \rangle^2] \geq 0, \end{aligned} \quad (3.9)$$

where the quantity $G^{\text{eff}} = G^{\text{eff}}(\beta, N, \bar{\sigma})$ is in general different from the shear modulus G in the Hamiltonian (3.4), depends on the temperature β , size N and external shear stress $\bar{\sigma}$, and could be identified as the macroscopic shear modulus measured in a laboratory. In addition, the entropy is given by the Gibbs–Shannon’s formula:

$$S = -k_B \sum_{s \in \Omega} p(s) \log p(s) = -\frac{\partial F}{\partial T}, \quad (3.10)$$

and the internal energy can be written as

$$U = \langle H(s) \rangle = \left\langle \sum_{i=1}^N \left\{ v_c \left[\frac{1}{2} G(\epsilon_i^e)^2 - \bar{\sigma} \epsilon_i \right] + \gamma(\epsilon_i^p) \xi_c \right\} \right\rangle + \langle H^{\text{int}}(s) \rangle. \quad (3.11)$$

A remark is in order here regarding the interpretation of the current statistical model that is specific to the elasto-plastic properties of solids. The thermodynamic relation (3.8) and the concavity of free energy (3.9) ($\bar{\sigma} \mapsto F(\beta, N, \bar{\sigma})$) are standard in a statistical model. However, when applying the free energy (3.7) for the prediction of the macroscopic response of an elasto-plastic body, we shall notice that plastic strain, once activated, is not recoverable; plastic processes, dissipating energy, are irreversible. To incorporate this feature, we separate the internal energy into four parts:¹⁴

$$\begin{aligned} U = \langle H(s) \rangle &= \left\langle \sum_{i=1}^N \left\{ v_c \left[\frac{1}{2} G(\epsilon_i^e)^2 - \bar{\sigma} \epsilon_i \right] + \gamma(\epsilon_i^p) \xi_c \right\} \right\rangle + \langle H^{\text{int}}(s) \rangle \\ &= U^{\text{el}} - \bar{\sigma} \bar{\epsilon} V + U^{\text{dsp}} + U^{\text{int}}, \end{aligned} \quad (3.12)$$

where

$$U^{\text{el}} = \left\langle \sum_{i=1}^N \left\{ v_c \left[\frac{1}{2} G(\epsilon_i^e)^2 \right] \right\} \right\rangle, \quad U^{\text{dsp}} = \left\langle \sum_{i=1}^N \left\{ \gamma(\epsilon_i^p) \xi_c \right\} \right\rangle, \quad U^{\text{int}} = \langle H^{\text{int}}(s) \rangle.$$

represents the elastic, dissipated, and interaction energy, respectively. Suppose that the interaction Hamiltonian $H^{\text{int}}(s)$ involves only plastic strain. We postulate that the macroscopic response of an elasto-plastic body is dictated by the total internal energy (3.12) in a monotonic loading process ($\bar{\sigma} \nearrow$) whereas the macroscopic response is governed only by the elastic part U^{el} of internal energy in a subsequent unloading process ($\bar{\sigma} \searrow$).

¹⁴ Similar decomposition can be done for the free energy once the interaction Hamiltonian is specified and will be useful for differentiating loading and unloading processes (Cf. (4.4)).

4. Noninteraction model (ideal plasticity)

In this section, we explore the implications of the statistical model outlined in the last section. Upon setting $H^{\text{int}}(s) \equiv 0$, we have a simplified non-interacting model, and the partition function for the system is given by

$$Z = Z_1^N,$$

where the partition function for a single site, by (3.1), can be written as

$$\begin{aligned} Z_1 &= \sum_{(\epsilon^e, \epsilon^p) \in \mathbb{S}} e^{-\beta \hat{H}(\epsilon^e, \epsilon^p; \bar{\sigma})} \\ &= \sum_{(\epsilon^e, \epsilon^p) \in \mathbb{S}} e^{-\beta \left\{ v_c \left[\frac{1}{2} G(\epsilon^e)^2 - \bar{\sigma} \epsilon \right] + \gamma(\epsilon^p) \xi_c \right\}} \\ &= \sum_{j \in \mathbb{Z}} e^{-\beta [\gamma(j \epsilon_*^p) \xi_c - j v_c \bar{\sigma} \epsilon_*^p]} \sum_{k \in \mathbb{Z}} e^{-\beta v_c \left[\frac{1}{2} G(k \epsilon_0)^2 - \bar{\sigma} (k \epsilon_0) \right]}. \end{aligned} \quad (4.1)$$

Converting the summation over $k \in \mathbb{Z}$ into an integral, we arrive at

$$Z_1^e = \frac{1}{\epsilon_0} \int_{\mathbb{R}} e^{-\beta v_c \left[\frac{1}{2} G(\epsilon^e)^2 - \bar{\sigma} \epsilon^e \right]} d\epsilon^e = \frac{1}{\epsilon_0} e^{\frac{\beta v_c \bar{\sigma}^2}{2G}} \sqrt{\frac{2\pi}{\beta v_c G}}. \quad (4.2)$$

Therefore, the partition function can be written as

$$Z_1 = Z_1^e Z_1^p, \quad Z_1^p := \sum_{j \in \mathbb{Z}} e^{-\beta [\gamma(j \epsilon_*^p) \xi_c - j v_c \bar{\sigma} \epsilon_*^p]}. \quad (4.3)$$

In other words, the partition function is simply the product of the partition function associated with elastic strain and that associated with plastic strain. Consequently, by (3.7), (4.2) and (4.8) the free energy is given by

$$F(\beta, N, \bar{\sigma}) = -k_B T \log(Z_1)^N =: F^{\text{el}}(\beta, N, \bar{\sigma}) + F^{\text{pl}}(\beta, N, \bar{\sigma}), \quad (4.4)$$

where

$$\begin{aligned} F^{\text{el}}(\beta, N, \bar{\sigma}) &= -k_B T N \log Z_1^e = -\frac{V \bar{\sigma}^2}{2G} - \frac{N}{2} k_B T \log T + \text{const.} \\ F^{\text{pl}}(\beta, N, \bar{\sigma}) &= -k_B T N \log Z_1^p. \end{aligned} \quad (4.5)$$

To proceed, we shall specify the form of the activation energy $\gamma = \gamma(\epsilon_p)$. As discussed in Section 2, the particular form of activation energy depends on the microscopic mechanisms of plastic strains and has to be postulated for the current statistical model as a constitutive relation.

To get some physical intuition, we first consider the minimum model with the plastic strain activation energy given by (2.3) with $c_1 = 0$. This minimum model will give rise to the familiar behavior of ideal plasticity and other thermo-elasto-plastic properties that are compared reasonably well with experiments. To see this, we notice that the partition function (4.3) associated with plastic strain for the minimum model, Z_1^p , can be written as

$$Z_1^p = 1 + \sum_{j=1}^{+\infty} e^{-j v_c \beta \epsilon_*^p \left(\frac{\gamma_0 \xi_c}{v_c \epsilon_*^p} - \bar{\sigma} \right)} + \sum_{j=-1}^{-\infty} e^{j v_c \beta \epsilon_*^p \left(\frac{\gamma_0 \xi_c}{v_c \epsilon_*^p} + \bar{\sigma} \right)}. \quad (4.6)$$

If

$$|\bar{\sigma}| < \sigma_Y := \frac{\gamma_0 \xi_c}{v_c \epsilon_*^p}, \quad (4.7)$$

the sums of an infinite geometric series in (4.6) can be analytically evaluated to obtain

$$\begin{aligned} Z_1^p &= 1 + \frac{1}{e^{\beta v_c \epsilon_*^p (-\bar{\sigma} + \sigma_Y)} - 1} + \frac{1}{e^{\beta v_c \epsilon_*^p (\bar{\sigma} + \sigma_Y)} - 1} \\ &= 1 + \frac{1}{e^{(1-\hat{\sigma})/\hat{T}} - 1} + \frac{1}{e^{(1+\hat{\sigma})/\hat{T}} - 1}, \end{aligned} \quad (4.8)$$

where the nondimensionalized temperature and applied stress are defined as

$$\hat{T} = \frac{k_B T}{v_c \epsilon_*^p \sigma_Y} = \frac{k_B T}{\gamma_0 \xi_c} \quad \text{and} \quad \hat{\sigma} = \frac{\bar{\sigma}}{\sigma_Y}. \quad (4.9)$$

The free energy of the system is given by (4.4) and (4.5) with the plastic part given by

$$F^{\text{pl}}(\beta, N, \bar{\sigma}) = -k_B T N \log \left[1 + \frac{1}{e^{(1-\hat{\sigma})/\hat{T}} - 1} + \frac{1}{e^{(1+\hat{\sigma})/\hat{T}} - 1} \right]. \quad (4.10)$$

The thermo-elastic-plastic properties of the sample are completely determined by a thermodynamic potential, e.g., the free energy (4.4). In particular, the strain-stress relation in the loading process, by (3.8), can be written as

$$\bar{\epsilon} = -\frac{1}{V} \frac{\partial F}{\partial \bar{\sigma}} = \bar{\epsilon}^e + \bar{\epsilon}^p, \quad (4.11)$$

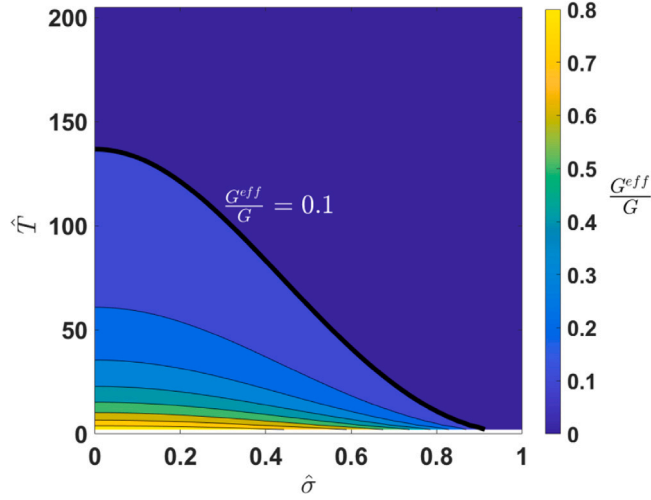


Fig. 4. Contours of $\frac{G^{\text{eff}}}{G}$ on $\hat{\sigma}$ - \hat{T} plane. The dark black line corresponds to $\frac{G^{\text{eff}}}{G} = 0.1$. The independent parameters for the non-interaction model are considered as $\xi_c = 2$ nm, $\sigma_Y = 79$ MPa, $e_*^p = 10^{-4}$, $G = 26$ GPa.

where the macroscopic elastic strain and plastic strain are given by

$$\begin{aligned}\bar{\epsilon}^e &= \sum_{k,j \in \mathbb{Z}} k \epsilon_0 \frac{e^{-\beta \left\{ v_c \left[\frac{1}{2} G(k\epsilon_0)^2 - \bar{\sigma} k \epsilon_0 \right] + \gamma (j e_*^p) \xi_c - \bar{\sigma} v_c j e_*^p \right\}}}{Z_1} = -\frac{1}{V} \frac{\partial F^{\text{el}}}{\partial \bar{\sigma}} = \frac{\bar{\sigma}}{G}, \\ \bar{\epsilon}^p &= \sum_{k,j \in \mathbb{Z}} j e_*^p \frac{e^{-\beta \left\{ v_c \left[\frac{1}{2} G(k\epsilon_0)^2 - \bar{\sigma} k \epsilon_0 \right] + \gamma (j e_*^p) \xi_c - \bar{\sigma} v_c j e_*^p \right\}}}{Z_1} = -\frac{1}{V} \frac{\partial F^{\text{pl}}}{\partial \bar{\sigma}} \\ &=: \epsilon_*^p \omega(\hat{\sigma}, \hat{T}).\end{aligned}\quad (4.12)$$

where $\omega(\hat{\sigma}, \hat{T})$ can be interpreted as the number of “plastons” induced by the (normalized) stress and temperature $(\hat{\sigma}, \hat{T})$, and is given by

$$\omega(\hat{\sigma}, \hat{T}) = \frac{\sinh(\hat{\sigma}/\hat{T})}{\cosh(1/\hat{T}) - \cosh(\hat{\sigma}/\hat{T})}. \quad (4.13)$$

“Plastons” can be thought of as hypothetical quasi-particles that get excited by applied stress or temperature to carry the flow of plastic deformation in the material (analogous to electron particles that get excited due to applied electric voltage to carry the flow of electric current in a conductor).

The macroscopic shear modulus defined by (3.9) can be written as

$$G^{\text{eff}}(T, \bar{\sigma}) = -V \left(\frac{\partial^2 F}{\partial \bar{\sigma}^2} \right)^{-1} = G \left[1 + \frac{G e_*^p}{\sigma_Y \hat{T}} \varphi(\hat{\sigma}, \hat{T}) \right]^{-1}, \quad (4.14)$$

where

$$\varphi(\hat{\sigma}, \hat{T}) = \frac{\cosh(1/\hat{T}) \cosh(\hat{\sigma}/\hat{T}) - 1}{(\cosh(1/\hat{T}) - \cosh(\hat{\sigma}/\hat{T}))^2}. \quad (4.15)$$

Moreover, the heat capacity associated with plastic strains at a constant applied stress $\bar{\sigma}$ is given by

$$C_{\bar{\sigma}} = -T \frac{\partial^2 F}{\partial T^2} = \frac{N}{2} k_B T - T \frac{\partial^2 F^{\text{pl}}}{\partial T^2}. \quad (4.16)$$

We fit the model with the experimental data for Aluminum (Carreker and Hibbard, 1957). We match the yield stress for Al (considered as stress corresponding to the strain of 0.5%) at 300 K using the model and experiment. The independent parameters for the non-interaction model are: $\xi_c = 2$ nm, $\sigma_Y = 79$ MPa, $e_*^p = 10^{-4}$, $G = 26$ GPa and $b = 0.286$ nm.

Fig. 4 shows plot of $\frac{G^{\text{eff}}}{G}$ on $\hat{\sigma}$ - \hat{T} plane obtained using (4.14). We observe that for a fixed temperature \hat{T} , the macroscopic shear modulus G^{eff} decreases as we increase the applied stress $\bar{\sigma}$, resulting in material yielding due to plastic deformation. Empirically, we may choose a threshold value of $\frac{G^{\text{eff}}}{G}$, e.g., 0.1, as the critical value indicating the sample would yield and collapse due to unconstrained plastic flow. The contour line corresponding to $\frac{G^{\text{eff}}}{G} = 0.1$ shown in Fig. 4 divides the $\hat{\sigma}$ - \hat{T} plane into two regions: lower region corresponds to the un-yielded phase, and the upper region corresponds to the yielded plastic phase. This phase transition observed at the macroscale is consistent with our postulate that “plasticity is a phase transition”.

The thermodynamic relations (4.11)–(4.16) are complicated and not amenable to physical interpretations in spite of being closed-form. To relate with the classical description of thermo-elastoplasticity, we explore a few regions on $\hat{\sigma}$ - \hat{T} plane where the predicted thermo-elastoplastic relations are particularly simple.

1. **Linear elasticity regime.** In the regime of low temperature and small applied stress, i.e.,

$$\hat{T} \ll 1 \quad \text{and} \quad 0 < \hat{\sigma} \ll 1, \quad (4.17)$$

by (4.12)–(4.13) and to the leading-order approximation, the plastic strain is given by

$$\frac{\bar{\epsilon}^p}{\epsilon_*^p} = \omega(\hat{\sigma}, \hat{T}) \approx \frac{\hat{\sigma}}{\hat{T}(\cosh(1/\hat{T}) - 1)} \ll 1. \quad (4.18)$$

Therefore, the strain–stress relation (4.11) is well approximated by the familiar Hooke's law:

$$\bar{\epsilon} = \bar{\epsilon}^e \quad \text{and} \quad \bar{\sigma} = G\bar{\epsilon}^e.$$

2. **Temperature-dependence of shear modulus.** The macroscopic shear modulus G^{eff} defined by (3.9) or (4.14) in general depends on the temperature, size, and applied stress. For simplicity, we consider the shear modulus at the zero applied stress:

$$G_0^{\text{eff}}(T) = -V \left(\frac{\partial^2 F}{\partial \bar{\sigma}^2} \right)^{-1} \Big|_{\bar{\sigma}=0} = G \left[1 + \frac{Gv_c(\epsilon_*^p)^2}{k_B T} \varphi(0, \hat{T}) \right]^{-1}.$$

where, by (4.25),

$$\varphi(0, \hat{T}) = \frac{1}{\cosh(1/\hat{T}) - 1} \approx 2e^{-1/\hat{T}},$$

and hence

$$G_0^{\text{eff}}(T) = \left(\frac{\partial \bar{\epsilon}}{\partial \bar{\sigma}} \right)^{-1} \Big|_{\bar{\sigma}=0} \approx G \left(1 + \frac{2Gv_c(\epsilon_*^p)^2}{k_B T} e^{-1/\hat{T}} \right)^{-1}.$$

3. **Melting temperature.** In the regime of high temperature and small applied stress, i.e.,

$$\hat{T} \gg 1 \quad \text{and} \quad 0 < \hat{\sigma} \ll 1, \quad (4.19)$$

by (4.14) we have

$$G_0^{\text{eff}}(T) = \left(\frac{\partial \bar{\epsilon}}{\partial \bar{\sigma}} \right)^{-1} \Big|_{\bar{\sigma}=0} = G \left[1 + \frac{Gv_c(\epsilon_*^p)^2}{k_B T} \varphi(0, \hat{T}) \right]^{-1} \approx G \left(1 + \frac{2Gk_B T}{\sigma_Y^2 v_c} \right)^{-1}.$$

Empirically, we may identify the melting temperature T_{melt} as the temperature such that $G_0^{\text{eff}}(T) \sim G/M_1$ for some large number M_1 , say, 10, i.e.,

$$\frac{2Gk_B T}{\sigma_Y^2 v_c} \sim M_1 \quad \Rightarrow \quad k_B T_{\text{melt}} \sim M_1 \frac{\sigma_Y^2 v_c}{2G}. \quad (4.20)$$

Experimentally, the melting temperature T_{melt} , yield stress σ_Y , and shear modulus (at $T = 0$) could be conveniently measured or extrapolated. Consequently, we could determine the size of element ξ_c as

$$\xi_c \sim \left(\frac{2Gk_B T_{\text{melt}}}{M_1 \sigma_Y^2} \right)^{1/3}.$$

Further,

$$\hat{T} = \frac{k_B T}{v_c \epsilon_*^p \sigma_Y} \sim \frac{T}{T_{\text{melt}}} M_1 \frac{\sigma_Y}{2G \epsilon_*^p}.$$

4. **Yield stress.** In the regime of large applied stress in the sense that

$$\beta v_c \epsilon_*^p (-\bar{\sigma} + \sigma_Y) = \frac{1 - \hat{\sigma}}{\hat{T}} \ll 1, \quad (4.21)$$

the plastic strain–stress relation (4.11) is well approximated by

$$\bar{\epsilon}^p = \epsilon_*^p \omega(\hat{\sigma}, \hat{T}) \approx \epsilon_*^p \left[\frac{\hat{T}}{1 - \hat{\sigma}} - \frac{1}{2} \coth(1/\hat{T}) + O\left(\frac{1 - \hat{\sigma}}{\hat{T}}\right) \right]. \quad (4.22)$$

Empirically, we may set the macroscopic temperature-dependent yield stress $\bar{\sigma}_Y$ as the applied stress such that $\bar{\epsilon}^p = 1/M_2$, $M_2 \sim 10^3$, i.e.,

$$\frac{\bar{\sigma}_Y(T)}{\sigma_Y} = 1 - M_2 \epsilon_*^p \hat{T} = 1 - M_1 M_2 \frac{\sigma_Y}{2G} \frac{T}{T_{\text{melt}}}. \quad (4.23)$$

5. **Flow stress.** In the regime (4.21) of large applied stress, from (4.14) we find the stress and temperature-dependent macroscopic shear modulus as

$$G^{\text{eff}}(\bar{\sigma}, T) = \left(\frac{\partial \bar{\epsilon}}{\partial \bar{\sigma}} \right)^{-1} \approx G \left[1 + \frac{Gv_c(\epsilon_*^p)^2 \hat{T}^2}{k_B T(1 - \hat{\sigma})} \right]^{-1}. \quad (4.24)$$

since

$$\varphi(\hat{\sigma}, \hat{T}) = \frac{\hat{T}^2}{1 - \hat{\sigma}} - \frac{1}{2} \hat{T} \coth(1/\hat{T}) + O\left(\frac{1 - \hat{\sigma}}{\hat{T}}\right). \quad (4.25)$$

Empirically, we may set the macroscopic flow stress $\bar{\sigma}_F$ as the applied stress such that ($M_3 \sim 10^2$)

$$\frac{G^{\text{eff}}(\bar{\sigma}_F, T)}{G} \sim \frac{1}{M_3} \quad \Rightarrow \quad \frac{Gv_c(\epsilon_*^p)^2 \hat{T}^2}{k_B T(1 - \hat{\sigma})} \sim M_3.$$

That is,

$$\frac{\bar{\sigma}_F(T)}{\sigma_Y} = 1 - \frac{1}{2} \frac{M_1}{M_3} \frac{T}{T_{\text{melt}}}. \quad (4.26)$$

In practice, both the macroscopic yield stress (4.23) and flow stress (4.26) are within 90% of σ_Y , and hence are regarded essentially as the same.

6. **Change of heat capacity in yield propagation.** The heat capacity can be obtained from the total free energy using (4.16). Recall the total free energy from (4.10) as,

$$F^{\text{pl}} = -k_B T N \log \left[1 + \frac{1}{e^{(1-\hat{\sigma})/\hat{T}} - 1} + \frac{1}{e^{(1+\hat{\sigma})/\hat{T}} - 1} \right].$$

- (i) In the regime (4.17) of low temperature $\hat{T} \ll 1$ and low applied stress $\hat{\sigma} \ll 1$,

$$F^{\text{pl}}(T, N, \bar{\sigma}) \approx -k_B T N \log \left[1 + 2e^{-1/\hat{T}} \right] \approx -2k_B T N e^{-1/\hat{T}}.$$

- (ii) In the regime of high temperature $\hat{T} \gg 1$ and zero applied stress $\hat{\sigma} \equiv 0$, we have

$$F^{\text{pl}} = -k_B T N \log \left[1 + \frac{2}{e^{1/\hat{T}} - 1} \right].$$

- (iii) In the regime (4.21) of low temperature $\hat{T} \ll 1$ and large applied stress $\bar{\sigma} > \bar{\sigma}_F$,

$$F^{\text{pl}}(T, N, \bar{\sigma}) = -k_B T N \log \left[1 + \frac{\hat{T}}{1 - \hat{\sigma}} \right].$$

The above derived quantities can be evaluated using the appropriate values for empirical parameters M_1, M_2, M_3 along with the model parameters fitted with the experimental data (as explained earlier to obtain Fig. 4). This also provides a way to verify the model with the experiments and simulations by comparing the observable quantities, such as shear modulus and melting temperature. From the above discussions, we see the minimum non-interacting model reproduces macroscopic phenomena of ideal plasticity that are quantitatively comparable with experimental data. The model could be enriched to include additional physical mechanisms such as strain/work hardening effects, strain softening effects, and effects of multiple slips system by considering more complex plastic strain activation energy $\gamma = \gamma(\epsilon^p)$, which will be briefly discussed in Appendix C.

5. Interaction model

In this section, we present the details of the interaction model. The non-interaction model, though reasonable, neglects quite a few important effects. To be specific, we assume the sample is sheared by applied traction on the top surface, as shown in Fig. 1. Because of geometric constraints and physical interaction, plastic strains at different spatial sites would interact with each other and interact with elastic strains. Possible microscopic mechanisms include interactions between various sources of plastic strains such as dislocations, dislocation loops, stacking faults, voids, inclusions of a second crystalline phase, etc. It is insurmountable to rigorously account for interactions between plastic strains from the first principles or an atomistic model. As a microscopic model, the plastic strain introduced here includes all inelastic non-recoverable strains in the process of deformation. In addition, from a statistical viewpoint, it is not unreasonable to postulate the interactions between plastic strains at two different sites are *homogeneous* and *isotropic* and hence, the interaction energy depends only on the distance between two sites:

$$H^{\text{int}}(\{\epsilon_i^p\}) = \frac{1}{2} \sum_{ij} J_{ij} \epsilon_i^p \epsilon_j^p, \quad (5.1)$$

where the interaction coefficients are given by

$$J_{ij} = J(|\mathbf{x}_i - \mathbf{x}_j|).$$

For ease of notion, define $J(0) = 0$ (instead of being singular). For reasonable physical behaviors, we require that

$$J_{ij} \geq 0 \quad \text{if } i \neq j,$$

meaning that interaction between two plastic strains of the same (resp. opposite) direction is repulsive (resp. attractive). We could include more terms in the Hamiltonian to account for interactions between elastic strains and plastic strains, and/or set the interaction coefficients J_{ij} as random variables. At this stage, we target at a minimum interaction model and focus on interactions between plastic strains at different sites for predictive modeling.

For brevity and future convenience, we introduce the number density $\rho(\mathbf{x})$ in quanta of ϵ_*^p , i.e., a smooth field $\rho = \rho(\mathbf{x})$ is such that

$$\epsilon_i^p = \epsilon_*^p v_c \rho(\mathbf{x}_i), \quad (5.2)$$

and denote by $\langle \bar{\epsilon}_i^p \rangle = \langle \epsilon_i^p \rangle = \epsilon_*^p \bar{\rho}(\mathbf{x}_i) v_c$

$$\begin{aligned} \phi_i &= \phi(\mathbf{x}_i) = \frac{1}{v_c} \sum_{j=1}^N J_{ij} \epsilon_j^p, \\ \bar{\phi}_i &= \langle \phi_i \rangle = \frac{1}{v_c} \sum_{j=1}^N J_{ij} \bar{\epsilon}_j^p = \epsilon_*^p \sum_{j=1}^N J_{ij} \bar{\rho}_j. \end{aligned} \quad (5.3)$$

Then we rewrite the interaction energy (5.1) as

$$\begin{aligned} H^{\text{int}} &= \frac{1}{2} \sum_{ij} J_{ij} \epsilon_i^p \epsilon_j^p = \frac{v_c}{2} \sum_i \epsilon_i^p \phi(\mathbf{x}_i) \\ &= \frac{v_c}{2} \sum_i (\epsilon_i^p - \bar{\epsilon}_i^p + \bar{\epsilon}_i^p) (\phi(\mathbf{x}_i) - \bar{\phi}(\mathbf{x}_i) + \bar{\phi}(\mathbf{x}_i)) \\ &= v_c \sum_i \left[\frac{1}{2} (\epsilon_i^p - \bar{\epsilon}_i^p) (\phi_i - \bar{\phi}_i) + \epsilon_i^p \bar{\phi}_i - \frac{1}{2} \bar{\epsilon}_i^p \bar{\phi}_i \right]. \end{aligned} \quad (5.4)$$

5.1. Mean-field approximation

For a mean-field approximation, we will neglect the first term on the right-hand side of (5.4), namely, the term pertaining to the fluctuation of the plastic strains at each site. The effective Hamiltonian within mean-field approximation can be written as (Cf. (3.2))

$$H^{\text{eff}}(s; \bar{\sigma}) = \sum_{i=1}^N \left\{ v_c \left[\frac{1}{2} G(\epsilon_i^e)^2 - \bar{\sigma} \epsilon_i^e \right] + \gamma (\epsilon_i^p) \xi_c - v_c \bar{\sigma}_i^{\text{eff}} \epsilon_i^p - \frac{1}{2} v_c \bar{\phi}_i \bar{\epsilon}_i^p \right\} \quad \forall s \in \Omega, \quad (5.5)$$

where the effective applied stress on the i th site is given by

$$\bar{\sigma}_i^{\text{eff}} = \bar{\sigma} - \bar{\phi}_i.$$

By similar calculations as in (4.1), we find the associated partition function as:

$$\begin{aligned} Z(\beta, N, \bar{\sigma}) &= \sum_{(\epsilon_1^e, \epsilon_1^p) \in \mathbb{S}} \dots \sum_{(\epsilon_N^e, \epsilon_N^p) \in \mathbb{S}} e^{-\beta H^{\text{eff}}(s; \bar{\sigma})} \\ &= \sum_{j \in \mathbb{Z}} \sum_{k \in \mathbb{Z}} \left[\prod_{i=1}^N e^{-\beta v_c \frac{1}{2} G(k\epsilon_0)^2 - \bar{\sigma}(k\epsilon_0)} \prod_{i=1}^N e^{\frac{1}{2} \beta v_c \bar{\phi}_i \bar{\epsilon}_i^p} e^{-\beta [\gamma (j\epsilon_0^p) \xi_c - j v_c \bar{\sigma}_i^{\text{eff}} \epsilon_i^p]} \right] \\ &= (Z_1^e)^N \left[\prod_{i=1}^N e^{\frac{1}{2} \beta v_c \bar{\phi}_i \bar{\epsilon}_i^p} Z_{1i}^p \right], \end{aligned} \quad (5.6)$$

where, in parallel to (4.3), (4.6), and (4.8), the partition function associated with the plastic strain at the i th site can be written (for the minimum model of ideal plasticity, i.e. $c_1 = 0$) as

$$\begin{aligned} Z_{1i}^p(\bar{\phi}_i; \bar{\sigma}, \beta) &= 1 + \sum_{j=1}^{+\infty} e^{-j v_c \beta \epsilon_*^p (\sigma_Y - \bar{\sigma}_i^{\text{eff}})} + \sum_{j=-1}^{-\infty} e^{j v_c \beta \epsilon_*^p (\sigma_Y + \bar{\sigma}_i^{\text{eff}})} \\ &= 1 + \frac{1}{e^{(1 - \bar{\sigma}_i^{\text{eff}})/\hat{T}} - 1} + \frac{1}{e^{(1 + \bar{\sigma}_i^{\text{eff}})/\hat{T}} - 1}. \end{aligned} \quad (5.7)$$

Once again, the free energy of the system is obtained as

$$F = -k_B T \log Z =: F^{\text{el}} + F^{\text{pl}},$$

where

$$F^{\text{pl}}(\{\bar{\phi}_i, \bar{\epsilon}_i\}; \beta, \bar{\sigma}) = \sum_{i=1}^N \left[-\frac{1}{2} v_c \bar{\phi}_i \bar{\epsilon}_i^p - k_B T \log Z_{1i}^p \right]. \quad (5.8)$$

Further, the average plastic strain at the i th site is given by (cf., (4.13))

$$\begin{aligned} \bar{\epsilon}_i^p &= \sum_{j \in \mathbb{Z}} j \epsilon_*^p \frac{e^{-\beta v_c j \epsilon_*^p (\text{sgn}(j) \sigma_Y - \bar{\sigma}_i^{\text{eff}})}}{Z_{1i}^p} = \frac{1}{v_c} \frac{\partial}{\partial \bar{\phi}_i} \left[-k_B T \log Z_{1i}^p(\bar{\phi}_i; \bar{\sigma}, \beta) \right] \\ &= \epsilon_*^p \omega(\bar{\sigma}_i^{\text{eff}}, \bar{T}), \end{aligned} \quad (5.9)$$

and the local strain–stress relation at the i th site is given by

$$\bar{\epsilon}_i = \bar{\epsilon}^e + \bar{\epsilon}_i^p, \quad \bar{\epsilon}^e = \frac{\bar{\sigma}}{G}.$$

Combining (5.9) with (5.3)₂, we can, in principle, determine the unknown $(\bar{\epsilon}_i^p, \bar{\phi}_i)$ in terms of the actual applied stress $\bar{\sigma}$ for self-consistency. Alternatively, Eqs. (5.3) and (5.9)₂ can be identified as the saddle point of the following function:

$$\Psi[\{\bar{\epsilon}_i, \bar{\phi}_i\}; \bar{\sigma}, \beta] = \sum_{i=1}^N \left[-k_B T \log Z_{1i}^p(\bar{\phi}_i; \bar{\sigma}, \beta) \right] + \frac{1}{2} \sum_{i,j=1}^N J_{ij} \bar{\epsilon}_i^p \bar{\epsilon}_j^p - v_c \sum_{i=1}^N \bar{\phi}_i \bar{\epsilon}_i^p, \quad (5.10)$$

whence

$$\begin{aligned} \frac{\partial}{\partial \bar{\phi}_i} \Psi[\{\bar{\epsilon}_i, \bar{\phi}_i\}; \bar{\sigma}, \beta] &= 0 \quad \Leftrightarrow \quad (5.9), \\ \frac{\partial}{\partial \bar{\epsilon}_i^p} \Psi[\{\bar{\epsilon}_i, \bar{\phi}_i\}; \bar{\sigma}, \beta] &= 0 \quad \Leftrightarrow \quad (5.3)_2, \end{aligned} \quad (5.11)$$

By (5.3)₂, we recognize the function $\Psi[\{\bar{\epsilon}_i, \bar{\phi}_i\}; \bar{\sigma}]$ in (5.10) is the free energy (5.8) in a different form. In addition, as a function of $\{\bar{\epsilon}_i, \bar{\phi}_i\}$, $\Psi[\{\bar{\epsilon}_i, \bar{\phi}_i\}; \bar{\sigma}, \beta]$ is strictly convex for each $\bar{\epsilon}_i$, and strictly concave for each $\bar{\phi}_i$ (Cf. (3.9)).

To proceed, it will be convenient to take a continuum viewpoint and convert the summations in (5.10) into integrals. Suppose that $D \subset \mathbb{R}^d$ is regular and summation in (5.3)₂ are over N -grid points in $D \cap \xi_c \mathbb{Z}^d$. Then, by (5.7) the single-sum terms in (5.10) can be approximated as

$$\begin{aligned} \sum_{i=1}^N \left[-k_B T \log Z_{1i}^p(\bar{\phi}_i; \bar{\sigma}, \beta) \right] &\longrightarrow F_*^{\text{pl}}[\bar{\phi}; \bar{\sigma}, \beta] := \\ &- \frac{k_B T}{v_c} \int_D \log \left[1 + \frac{1}{e^{(1-\bar{\sigma}^{\text{eff}})/\bar{T}} - 1} + \frac{1}{e^{(1+\bar{\sigma}^{\text{eff}})/\bar{T}} - 1} \right] \quad \left(\bar{\sigma}^{\text{eff}} = \frac{\bar{\sigma} - \bar{\phi}}{\sigma_Y} \right), \end{aligned} \quad (5.12)$$

and (recall that $\bar{\epsilon}_i^p = v_c \epsilon_*^p \bar{\rho}(\mathbf{x}_i)$)

$$v_c \sum_{i=1}^N \bar{\phi}_i \bar{\epsilon}_i^p \longrightarrow v_c \epsilon_*^p \int_D \bar{\phi} \bar{\rho}. \quad (5.13)$$

For the double-sum interaction term in (5.10), i.e., $\frac{1}{2} \sum_{i,j=1}^N J(\mathbf{x}_i - \mathbf{x}_j) \bar{\epsilon}_i^p \bar{\epsilon}_j^p$, we can convert it into a bilinear form as follows:

$$\frac{1}{2} \sum_{i,j=1}^N J(\mathbf{x}_i - \mathbf{x}_j) \bar{\epsilon}_i^p \bar{\epsilon}_j^p \longrightarrow \langle H^{\text{int}} \rangle[\bar{\rho}] = \frac{1}{2} \int_D \bar{\rho} \mathcal{A}[\bar{\rho}], \quad (5.14)$$

where $\mathcal{A}[\]$ is a self-adjoint linear operator that is dictated by the interaction potential $J(\mathbf{x})$ and will be explicitly calculated later. Consequently, by (5.12)–(5.14) the variational principle corresponding to (5.10) in the continuum setting can be written as

$$\min_{\bar{\rho}} \max_{\bar{\phi}} \Psi_*[\bar{\rho}, \bar{\phi}; \bar{\sigma}, \beta], \quad \Psi_*[\bar{\rho}, \bar{\phi}; \bar{\sigma}, \beta] = F_*^{\text{pl}}[\bar{\phi}; \bar{\sigma}, \beta] + \langle H^{\text{int}} \rangle[\bar{\rho}] - v_c \epsilon_*^p \int_D \bar{\phi} \bar{\rho}. \quad (5.15)$$

From von Neumann’s min–max theorem (Neumann, 1928), the solution to the above problem exists and is unique since the functional is strictly concave with respect to $\bar{\phi}$ and strictly convex with respect to $\bar{\rho}$.

5.2. Interaction law

In this section, we provide the rationale for using the interaction potential among microscopic elasto-plastic units as a power law. The interactions among two parallel dislocation lines spaced by a distance $|\mathbf{x}|$ in a plastically deforming body are of the logarithmic form $(\log |\mathbf{x}|)$. Our microscopic model is, however, coarser than the scale of dislocations, and as such, we may consider interacting inclusions with a plastic eigenstrain. While the interaction between two isolated inclusions in an infinite linear elastic media is well-defined $(1/|\mathbf{x}|^2)$, the exact interaction with multiple such inclusions (that accounts for screening), a surrounding matrix that is itself deforming plastically and with possible image forces due to boundaries, is unknown. In addition, we expect processing conditions to also influence this interaction. In other words, while it is hard to pin down the exact interaction law, a power law is a reasonable proposal in the form of $(1/|\mathbf{x}|^\alpha)$ for the pair-wise interactions among elasto-plastic units, where α is a phenomenological parameter that allows varying the qualitative nature of the interactions. Specifically, the pair-wise interaction potential $J(\mathbf{x})$ is specified as a two-piece function with the long-range interaction being a power law:

$$J(\mathbf{x}) = \begin{cases} J_{\text{core}}(\mathbf{x}) & \text{if } |\mathbf{x}| < C \xi_c, \\ \frac{A_\alpha}{|\mathbf{x}|^\alpha} & \text{if } |\mathbf{x}| \geq C \xi_c, \end{cases} \quad (5.16)$$

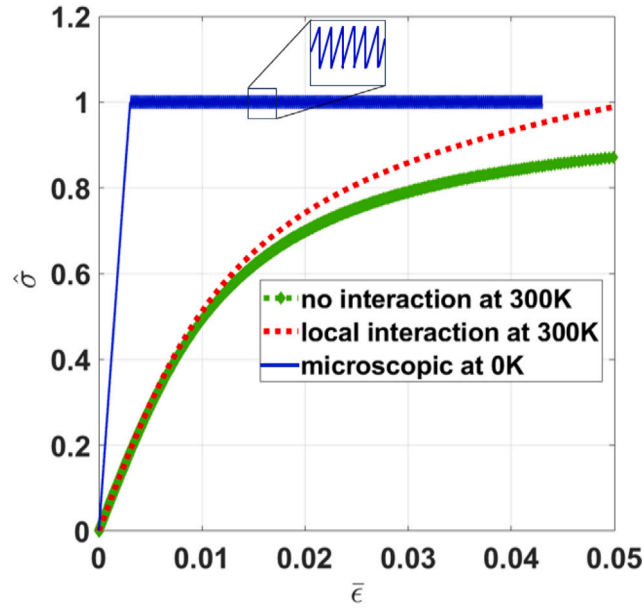


Fig. 5. Elasto-plastic behavior for microscopic, no interaction and local interaction case. The independent parameters for the non-interaction model are considered as $\xi_c = 2$ nm, $\sigma_Y = 79$ MPa, $\epsilon_*^p = 10^{-4}$, $G = 26$ GPa and $b = 0.286$ nm. The independent parameters in the local interaction case are considered as $q = 4$, $\alpha = 4.5$ and A_α is chosen by setting $\frac{qA_\alpha}{(\epsilon_*^p)^2} = 100$ MPa.

where $0 < C < 1$ is a constant, and $A_\alpha > 0$ reflects the strength of the long-range interaction and will be specified later. The core interaction potential $J_{\text{core}}(\mathbf{x})$ can, in principle, be calculated from a specified microscopic interaction mechanism. However, we do not expect the local core interaction potential $J_{\text{core}}(\mathbf{x})$ would affect the size-dependent properties of a body. Since our main focus in this work lies in the nonlocal effect of long-range interactions, we neglect the core interaction potential and set $J_{\text{core}}(\mathbf{x}) \equiv 0$.

Depending on the exponent α , there are three regimes of interactions that should be treated differently, as explained in the following sections.

5.3. Local interaction

First, we consider the case of local interaction. If $\alpha > d + 2$, the terms in (5.14) decay fast as $|\mathbf{x}_j - \mathbf{x}_i|$ increases. Therefore, it suffices to consider “nearest-neighbor” interactions. Let \mathcal{N}_i denote pairs of nearest-neighbors. Then (5.14) may be approximated by

$$\bar{\phi}(\mathbf{x}_i) \approx \frac{1}{v_c} \sum_{j \in \mathcal{N}_i} J(\mathbf{x}_i - \mathbf{x}_j) \bar{\epsilon}_j^p \approx \frac{q \epsilon_*^p A_\alpha}{\xi_c^\alpha} \bar{\rho}(\mathbf{x}_i), \tag{5.17}$$

where q is the number of nearest neighbors for an interior grid point, and the last line follows from the assumption that the average density $\bar{\rho} = \bar{\rho}(\mathbf{x})$ does not vary significantly over the lengthscale ξ_c . Moreover, the average interaction energy can be approximated as

$$\langle H^{\text{int}} \rangle[\bar{\epsilon}^p] = \frac{1}{2} \sum_{i,j=1}^N J(\mathbf{x}_i - \mathbf{x}_j) \bar{\epsilon}_i^p \bar{\epsilon}_j^p = \frac{v_c}{2} \sum_{i=1}^N \bar{\phi}_i \bar{\epsilon}_i^p \rightarrow \frac{v_c q (\epsilon_*^p)^2 A_\alpha}{2 \xi_c^\alpha} \int_D \bar{\rho}^2 d\mathbf{x}. \tag{5.18}$$

Therefore, the Euler–Lagrange’s equation associated with the variational problem (5.15), or equivalently, the continuum field equations corresponding to (5.11) can be written as (cf., (4.13))

$$\begin{cases} v_c \bar{\rho} = \omega \left(\frac{\bar{\sigma} - \bar{\phi}}{\sigma_Y}, \hat{T} \right), \\ \bar{\phi} = \frac{q \epsilon_*^p A_\alpha}{\xi_c^\alpha} \bar{\rho}. \end{cases} \tag{5.19}$$

We combine the two self-consistent equations in (5.19) into one non-linear equation and solve it explicitly. Fig. 5 shows the obtained macroscopic elasto-plastic response for the local interaction case. We observe that for a uniform applied stress $\bar{\sigma}$, the solution for the local interaction case is uniform with no size-effect. The flow stress for the local interaction in Fig. 5 is observed to be higher than in the non-interaction case. This higher flow stress for the local interaction is caused by the repulsive interactions among plastic strains at different elements that would resist the plastic flow, effectively resulting in strain hardening.

5.4. Nonlocal interaction

Next, we consider a long-range interaction case that gives rise to a nonlocal coarse-grained model. Suppose that the power law exponent $\alpha = d + 2s \in (d, d + 2)$ for some $s \in (0, 1)$. By (5.16) we have

$$\begin{aligned} \bar{\phi}(\mathbf{x}_i) &= \frac{1}{v_c} \sum_{j=1}^N J(\mathbf{x}_i - \mathbf{x}_j) \bar{\epsilon}_i^p + \frac{1}{v_c} \sum_{j=1}^N J(\mathbf{x}_i - \mathbf{x}_j) (\bar{\epsilon}_j^p - \bar{\epsilon}_i^p) \\ &\approx \kappa_D(\mathbf{x}_i) \epsilon_*^p \bar{\rho}(\mathbf{x}_i) + \frac{\Lambda_\alpha \epsilon_*^p}{v_c} \int_D \frac{\bar{\rho}(\mathbf{y}) - \bar{\rho}(\mathbf{x}_i)}{|\mathbf{y} - \mathbf{x}_i|^{d+2s}} d\mathbf{y}, \end{aligned} \tag{5.20}$$

where

$$\kappa_D(\mathbf{x}) = \sum_{j=1}^N J(\mathbf{x}_j - \mathbf{x}) \approx \sum_{\mathbf{x}_j \in D \cap \xi_c \mathbb{Z}^d} J(\mathbf{x}_j - \mathbf{x}),$$

and the integral in (5.20)₂ is conditionally integrable over a bounded domain and should be interpreted in the sense of ‘‘Principal Value’’ (P.V.). We recall the definition of fractional Laplace operators (see Appendix A). Upon smoothly extending $\bar{\rho}(\mathbf{x})$ to \mathbb{R}^d by zero, we rewrite (5.20) as $(\Lambda'_\alpha = \Lambda_\alpha/v_c C(d, s))$

$$\bar{\phi}(\mathbf{x}) = \epsilon_*^p \left[\kappa_D(\mathbf{x}) \bar{\rho}(\mathbf{x}) - \Lambda'_\alpha (-\Delta)^s \bar{\rho}(\mathbf{x}) \right], \tag{5.21}$$

and the average interaction energy is identified as

$$\langle H^{\text{int}} \rangle[\bar{\rho}] = \frac{v_c (\epsilon_*^p)^2}{2} \left[\int_{\mathbb{R}^d} \kappa_D(\mathbf{x}) \bar{\rho}^2(\mathbf{x}) d\mathbf{x} - \Lambda'_\alpha \int_{\mathbb{R}^d} \bar{\rho}(\mathbf{x}) (-\Delta)^s \bar{\rho}(\mathbf{x}) d\mathbf{x} \right]. \tag{5.22}$$

Therefore, the Euler–Lagrange’s equation associated with the variational problem (5.15), or equivalently, the continuum field equations corresponding to (5.11) can be written as

$$\begin{cases} v_c \bar{\rho} = \omega \left(\frac{\bar{\sigma} - \bar{\phi}}{\sigma_Y}, \hat{T} \right), \\ \bar{\phi} = \epsilon_*^p \kappa_D(\mathbf{x}) \bar{\rho}(\mathbf{x}) - \epsilon_*^p \Lambda'_\alpha (-\Delta)^s \bar{\rho}(\mathbf{x}). \end{cases} \tag{5.23}$$

From (4.13), we recognize that (5.23)₁ defines a monotonic map

$$\frac{\bar{\sigma} - \bar{\phi}}{\sigma_Y} \mapsto \bar{\rho},$$

which can be inverted, giving rise to the inverse function:

$$\frac{\bar{\sigma} - \bar{\phi}}{\sigma_Y} = m(\bar{\rho}). \tag{5.24}$$

Here, we omit the \hat{T} -dependence for brevity and emphasize that the function $m : \mathbb{R} \rightarrow \mathbb{R}$ is analytic, independent of the domain D , and monotonically increases from $m(0) = 0$ to $m(\bar{\rho}) \rightarrow 1$ as $\bar{\rho} \rightarrow +\infty$ (Cf. (4.13)). Inserting (5.24) into (5.23)₂ we obtain

$$\underbrace{-\epsilon_*^p \Lambda'_\alpha (-\Delta)^s \bar{\rho} + \epsilon_*^p \kappa_D(\mathbf{x}) \bar{\rho}}_{=\bar{\phi}, \text{ arising from nonlocal interactions}} + \sigma_Y m(\bar{\rho}) = \bar{\sigma} \quad \text{in } D, \tag{5.25}$$

which is equivalent to the outer minimization problem in (5.15). That is, the following variational problem:

$$\min_{\bar{\rho}} \Psi_*[\bar{\rho}, \bar{\phi}; \bar{\sigma}, \beta] = \min_{\bar{\rho}} \left\{ \langle H^{\text{int}} \rangle[\bar{\rho}] + v_c \epsilon_*^p \int_D (\sigma_Y M(\bar{\rho}) - \bar{\sigma} \bar{\rho}) d\mathbf{x} \right\}, \tag{5.26}$$

where the function $M : \mathbb{R} \rightarrow \mathbb{R}$ is an anti-derivative of $m : \mathbb{R} \rightarrow \mathbb{R}$, i.e., $dM(\bar{\rho})/d\bar{\rho} = m(\bar{\rho})$.

Size effect analysis. We now analyze the effects of nonlocal interaction, particularly on the size-dependent flow stress. We now consider the flow stress as determined by (5.23) or (5.26). As discussed in Section 4, the flow stress can be identified either by certain threshold plastic strain or macroscopic shear modulus. For instance, we choose threshold value (denoted by $\bar{\epsilon}_{\text{th}}^p$) of average plastic strain of the entire sample as the criterion for identifying the flow stress, i.e., $\bar{\sigma}_F$ is such that the solution to (5.23) or (5.26) satisfies that

$$\frac{1}{|D|} \int_D \bar{\epsilon}_*^p \bar{\rho}(\mathbf{x}) = \bar{\epsilon}_{\text{th}}^p. \tag{5.27}$$

Suppose that the size of D is of order one (~ 1) and the threshold plastic strain distribution, as a solution to (5.23) or (5.26), is denoted by $\bar{\rho}^*(\mathbf{x})$. By (5.24), we find that the flow stress for the body D is given by

$$\bar{\sigma}_F = \frac{1}{|D|} \int_D \left[\sigma_Y m(\bar{\rho}^*) + \bar{\phi}[\bar{\rho}^*] \right], \tag{5.28}$$

where $\frac{1}{|D|} \int_D m(\bar{\rho}^*) \sim 1$. For a body of different size, i.e., we consider a transformation of the body:

$$D \rightarrow D_\lambda = \lambda D = \{ \mathbf{y} : \mathbf{y} = \lambda \mathbf{x}, \mathbf{x} \in D \}. \tag{5.29}$$

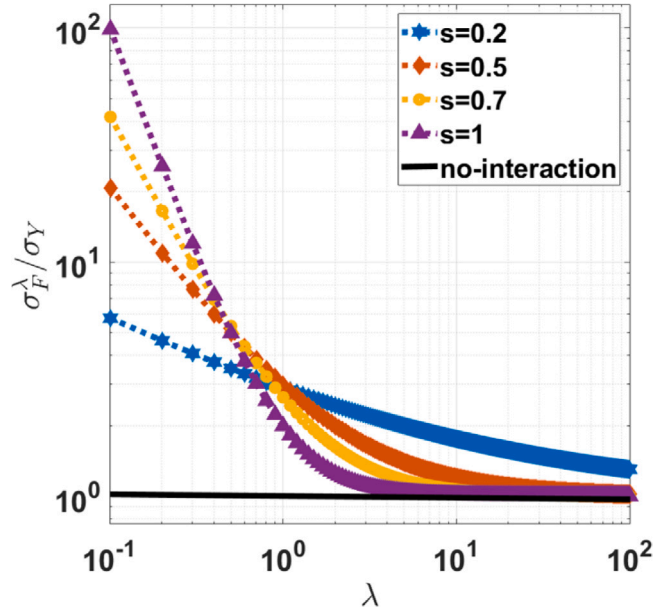


Fig. 6. Normalized flow stress for different size scale parameters λ (log–log plot). For plotting, the size scale parameter λ in (5.33) is modified as $(s\lambda)$ to improve the visibility of different plots in the figure. For simplicity, the constant of proportionality in (5.33) is chosen as unity.

To keep consistency with (5.27), we anticipate that the threshold plastic strain distribution would transform as

$$\bar{\rho}^*(\mathbf{x}) \rightarrow \bar{\rho}_\lambda^*(\mathbf{y}) = \bar{\rho}^*(\mathbf{y}/\lambda) = \bar{\rho}^*(\mathbf{x}) \quad \forall \mathbf{y} \in D_\lambda. \quad (5.30)$$

From the discussion in Appendix, the conjugate stress shall transform as

$$\bar{\phi}[\bar{\rho}^*](\mathbf{x}) \rightarrow \bar{\phi}_\lambda[\bar{\rho}_\lambda^*](\mathbf{y}) = \lambda^{-2s} \bar{\phi}[\bar{\rho}^*](\mathbf{y}/\lambda) = \lambda^{-2s} \bar{\phi}[\bar{\rho}^*](\mathbf{x}). \quad (5.31)$$

From (5.25) and (5.28) we conclude that the flow stress should transform as

$$\begin{aligned} \bar{\sigma}_F \rightarrow \bar{\sigma}_F^\lambda &= \frac{1}{|D_\lambda|} \int_{D_\lambda} [\sigma_Y m(\bar{\rho}_\lambda^*) + \bar{\phi}_\lambda[\bar{\rho}_\lambda^*]] = \frac{\lambda^d}{|D_\lambda|} \int_D [\sigma_Y m(\bar{\rho}^*) + \lambda^{-2s} \bar{\phi}[\bar{\rho}^*]] \\ &= \frac{1}{|D|} \int_D [\sigma_Y m(\bar{\rho}^*) + \lambda^{-2s} \bar{\phi}[\bar{\rho}^*]]. \end{aligned} \quad (5.32)$$

At a macroscopic scale when $\lambda \gg 1$, (5.32) implies that the flow stress is given by

$$\bar{\sigma}_F^\infty = \sigma_Y \frac{1}{|D|} \int_D m(\bar{\rho}^*) \approx \sigma_Y.$$

Inserting the above equation into (5.32), we have

$$\frac{\bar{\sigma}_F^\lambda - \bar{\sigma}_F^\infty}{\bar{\sigma}_F^\infty} \propto \lambda^{-2s}. \quad (5.33)$$

Fig. 6 shows the normalized flow stress ($\bar{\sigma}_F^\lambda / \sigma_Y$) with non-local interactions as the size scale parameter λ is varied. We observe that the relative change in the flow stress decays with the size scale parameter λ as a power law, and it asymptotically converges to the flow stress for the non-interaction case (σ_Y) as $\lambda \rightarrow \infty$. The variation in flow stress is higher for smaller sizes (i.e. small λ). This indicates that the size effect is more dominant at smaller length scales, as observed in the experiments.

The higher flow stress for a smaller size scale (i.e. smaller λ) is a consequence of non-local interactions among the plastic strains, i.e., the nonlocal interaction energy (5.22) (Cf. (B.7)):

$$\langle H^{int}[\bar{\epsilon}^p] \rangle \propto \int_D \int_D \frac{\bar{\epsilon}^p(\mathbf{x}) \bar{\epsilon}^p(\mathbf{y})}{|\mathbf{x} - \mathbf{y}|^{d+2s}} d\mathbf{x} d\mathbf{y}. \quad (5.34)$$

We recall that in Dahlberg and Ortiz (2019) the non-local fractional plastic strain-gradient contribution Ψ_g to the free energy is prescribed as:

$$\Psi_g(\bar{\epsilon}^p) \propto \int_D \int_D \frac{|\bar{\epsilon}^p(\mathbf{x}) - \bar{\epsilon}^p(\mathbf{y})|^{n+1}}{|\mathbf{x} - \mathbf{y}|^{d+s(n+1)}} d\mathbf{x} d\mathbf{y}. \quad (5.35)$$

If the non-local hardening exponent $n = 1$, the two energy forms in (5.34)–(5.35) admit the same scaling with respect to the transformation $D \rightarrow D_\lambda = \lambda D$ and $\bar{\epsilon}^p \rightarrow \bar{\epsilon}_\lambda^p(\mathbf{y}) = \bar{\epsilon}^p(\mathbf{y}/\lambda)$:

$$(\langle H^{int}[\bar{\epsilon}^p] \rangle, \Psi_g(\bar{\epsilon}^p)) \rightarrow \lambda^{d-2s} (\langle H^{int}[\bar{\epsilon}^p] \rangle, \Psi_g(\bar{\epsilon}^p)).$$

Therefore, the two models would yield the same scaling law (5.33) for the size-dependent flow stress. In present work, we provide a plausible microscopic origin for the exponent s from the long-range nonlocal power-law interactions among the plastically deforming microscopic units. Thus, in a nutshell, the emergent fractional size scaling in plasticity at the macroscale is dictated by the non-local interactions among the plastically deforming microscopic units.

5.5. Screening long-range interaction

If $\alpha = d - 2s < d$ for some $s > 0$, we identify (5.3)₂ as a negative fractional operator (see Appendix B):

$$\bar{\phi}(\mathbf{x}_i) = \frac{1}{v_c} \sum_{j=1}^N J(\mathbf{x}_i - \mathbf{x}_j) \bar{\epsilon}_j^p \approx \frac{c_*^p \Lambda_\alpha}{v_c} \int_D \frac{\bar{\rho}(\mathbf{y})}{|\mathbf{y} - \mathbf{x}_i|^{d-2s}} d\mathbf{y} = \frac{c_*^p \Lambda_\alpha}{v_c B(d, s)} (-\Delta)^{-s} \bar{\rho}(\mathbf{x}_i). \quad (5.36)$$

In addition, the average interaction energy is identified as

$$\langle H^{int} \rangle[\bar{\rho}] = \frac{\Lambda_\alpha (c_*^p)^2}{2B(d, s)} \int_{\mathbb{R}^d} \bar{\rho}(\mathbf{x}) (-\Delta)^{-s} \bar{\rho}(\mathbf{x}) d\mathbf{x}. \quad (5.37)$$

Therefore, the Euler–Lagrange’s equation associated with the variational problem (5.15), or equivalently, the continuum field equations corresponding to (5.11) can be written as

$$\begin{cases} v_c \bar{\rho} = \omega \left(\frac{\bar{\sigma} - \bar{\phi}}{\sigma_Y}, \hat{T} \right), \\ \bar{\phi} = \frac{(c_*^p)^2 \Lambda_\alpha}{v_c B(d, s)} (-\Delta)^{-s} \bar{\rho} \iff -\Delta^s \bar{\phi} = \frac{(c_*^p)^2 \Lambda_\alpha}{v_c B(d, s)} \bar{\rho}. \end{cases} \quad (5.38)$$

Screening effect analysis. We now analyze the implications of (5.38). Inserting (5.38)₂ into (5.38)₁, we obtain ($l^{2s} = \sigma_Y v_c^2 B(d, s) / (c_*^p)^2 \Lambda_\alpha$ and $\alpha = d - 2s$)

$$-l^{2s} \Delta^s \bar{\phi} = \sigma_Y \omega \left(\frac{\bar{\sigma} - \bar{\phi}}{\sigma_Y}, \hat{T} \right) \quad \text{in } D, \quad (5.39)$$

which is again equivalent to the outer minimization problem in (5.15) or the following variational problem:

$$\min_{\bar{\rho}} \Psi_*[\bar{\rho}, \bar{\phi}; \bar{\sigma}, \beta] = \min_{\bar{\rho}} \left\{ \langle H^{int} \rangle[\bar{\rho}] + v_c c_*^p \int_D (\sigma_Y M(\bar{\rho}) - \bar{\sigma} \bar{\rho}) d\mathbf{x} \right\}. \quad (5.40)$$

In particular, as $s \rightarrow 1-$ we have

$$\bar{\phi}(\mathbf{x}) = \lim_{s \rightarrow 1-} \frac{(c_*^p)^2 \Lambda_\alpha}{v_c B(d, s)} (-\Delta)^{-s} \bar{\rho}(\mathbf{x}) \propto \begin{cases} \int_{\mathbb{R}^d} \frac{\bar{\rho}(\mathbf{y})}{|\mathbf{x} - \mathbf{y}|^{d-2}} d\mathbf{y} & \text{if } d \neq 2, \\ \int_{\mathbb{R}^2} \bar{\rho}(\mathbf{y}) \log |\mathbf{x} - \mathbf{y}| d\mathbf{y} & \text{if } d = 2, \end{cases} \quad (5.41)$$

and rewrite (5.39) as

$$-l^2 \Delta \bar{\phi} = \sigma_Y \omega \left(\frac{\bar{\sigma} - \bar{\phi}}{\sigma_Y}, \hat{T} \right) \quad \text{in } D. \quad (5.42)$$

Since $\hat{\sigma} \mapsto \omega(\hat{\sigma}, \hat{T})$ is monotonically increasing, the above equation implies a screening or boundary-layer feature in the sense that $\bar{\phi}$ is almost uniform and equal to $\bar{\sigma}$ in the interior of the body D except for a boundary layer of thickness $\sim l$ close to the surface ∂D . Such a solution implies that $\bar{\rho} = 0$ (i.e., plastic strain $\bar{\epsilon}^p = 0$) except in the boundary layer. In other words, the “strong” long-range repulsive interaction implies plastic strains can only be generated within a boundary layer of thickness $\sim l$.

6. Concluding remarks

We briefly take stock of what we have accomplished, and perhaps equally important, what has been left unsaid. Starting with a rather bare-bones microscopic picture of interacting material units that yield at slightly different stages, we show that statistical mechanics provides an effective coarse-graining strategy to emerge with a macroscopic continuum descriptor. The most significant novelty of our work is that we show the precise microscopic interaction conditions that will lead to the various flavors of plasticity theories; be it classical plasticity or a fractional strain gradient plasticity. To our knowledge, our work is the first to infer an emergent continuum fractional type theory for plasticity by invoking statistical mechanics. Finally, our work provides a microscopic connection to the experimentally observed size-effects.

What we do not do (or are unable to do) is to connect our work directly with dislocations. In that sense, our modeling approach is no less phenomenological than continuum strain gradient plasticity (or the fractional version by Dahlberg and Ortiz). The mathematical problem underpinning the coarse-graining of dislocation (along the lines of what we have done here) is formidable.

Aside from bridging this gap, the developed theory can be further extended to explicitly account for time and rate dependency using the principles of non-equilibrium statistical mechanics (Leadbetter et al., 2023; Huang et al., 2022; Kulkarni, 2023). Finally, another exciting future direction is to perform an in-depth study of "plastons" introduced in this work to be the fundamental carrier of plasticity in the material. For example, investigating the laws that govern the plastons would possibly allow us to use them to alternately model time-dependent plastic flow using frameworks such as non-equilibrium statistical mechanics.

We note that the key results we derived in the interaction case, such as the derivation of fractional nonlocal continuum equations and the size effect analysis, are based on the energy function Ψ in (5.15) that we constructed. This construction mainly depends on the analytical response function of the system for known loading; in this work, we derived (5.9) as the macroscopic plastic strain response to the applied stress $\bar{\sigma}$, mean field of interaction ($\bar{\phi}$), and temperature T using statistical mechanics. We note that the procedure outlined in this work can be extended to derive the fractional nonlocal continuum equations and the size effect analysis for other fields, such as electrostatics. First, one has to arrive at the final response function of the system in an analytical form for known loading and mean field of interaction (similar to (5.9) in this work) using any techniques, such as statistical mechanics. Then, the derivation of fractional nonlocal continuum equations and the size effect analysis would follow from the procedure we presented in Section 5. We note that our choice of statistical mechanics, in particular, allowed us to introduce temperature as the key parameter in studying plasticity.

CRedit authorship contribution statement

Pratik Khandagale: Writing – review & editing, Writing – original draft, Methodology, Investigation, Formal analysis. **Liping Liu:** Writing – review & editing, Writing – original draft, Supervision, Methodology, Investigation, Formal analysis. **Pradeep Sharma:** Writing – review & editing, Writing – original draft, Supervision, Resources, Methodology, Investigation, Funding acquisition, Conceptualization.

Declaration of competing interest

The authors declare that they have no known competing financial interests or personal relationships that could have appeared to influence the work reported in this paper.

Data availability

No data was used for the research described in the article.

Acknowledgment

P.S. gratefully acknowledges helpful comments from Professors Kaushik Dayal, Alan Needleman and the support of the Hugh Roy and Lillie Cranz Cullen Distinguished University Chair from the University of Houston. L.L. gratefully acknowledges the support of NSF DMS-2306254 and Simons travel grant.

Appendix A. Fractional Laplacians

Let $u : \mathbb{R}^d \rightarrow \mathbb{R}$ be a smooth function with all of its derivatives converging to zero at infinity (more precisely, a tempered distribution). For $s \in (0, 1)$, the positive and negative fractional Laplace operators are defined as Di Nezza et al. (2012)

$$\begin{aligned} (-\Delta)^s u(\mathbf{x}) &= C(d, s) \text{P.V.} \int_{\mathbb{R}^d} \frac{u(\mathbf{x}) - u(\mathbf{y})}{|\mathbf{x} - \mathbf{y}|^{d+2s}} d\mathbf{y}, \\ (-\Delta)^{-s} u(\mathbf{x}) &= B(d, s) \int_{\mathbb{R}^d} \frac{u(\mathbf{y})}{|\mathbf{x} - \mathbf{y}|^{d-2s}} d\mathbf{y}, \end{aligned} \quad (\text{A.1})$$

where the principal value and constants $C(d, s)$ and $B(d, s)$ are defined as

$$\begin{aligned} \text{P.V.} \int_{\mathbb{R}^d} \frac{u(\mathbf{x}) - u(\mathbf{y})}{|\mathbf{x} - \mathbf{y}|^{d+2s}} d\mathbf{y} &= \lim_{\epsilon \rightarrow 0} \int_{\mathbb{R}^d \setminus B_\epsilon(\mathbf{x})} \frac{u(\mathbf{x}) - u(\mathbf{y})}{|\mathbf{x} - \mathbf{y}|^{d+2s}} d\mathbf{y}, \\ C(d, s) &= \left(\int_{\mathbb{R}^d} \frac{1 - \cos z_1}{|z|^{d+2s}} dz \right)^{-1}, \quad B(d, s) = \left(\int_{\mathbb{R}^d} \frac{\cos z_1}{|z|^{d-2s}} dz \right)^{-1}. \end{aligned} \quad (\text{A.2})$$

Fractional Laplace operators enjoy some neat properties as the usual Laplacian $-\Delta$ or inverse Laplacian $-\Delta^{-1}$. In particular, we have

$$\begin{aligned} \lim_{s \rightarrow 1^-} (-\Delta)^s u(\mathbf{x}) &= -\Delta u(\mathbf{x}), & \lim_{s \rightarrow 0^+} (-\Delta)^s u(\mathbf{x}) &= u(\mathbf{x}), \\ \lim_{s \rightarrow 1^-} (-\Delta)^{-s} u(\mathbf{x}) &= -\Delta^{-1} u(\mathbf{x}), & \lim_{s \rightarrow 0^+} (-\Delta)^{-s} u(\mathbf{x}) &= u(\mathbf{x}). \end{aligned}$$

Further, we have

$$(-\Delta)^{-s} (-\Delta)^s u(\mathbf{x}) = (-\Delta)^s (-\Delta)^{-s} u(\mathbf{x}) = u(\mathbf{x}) \quad \forall s \in (0, 1). \quad (\text{A.3})$$

To see this, we notice that, upon a change of variables $\mathbf{y} \rightarrow \mathbf{z} = \mathbf{y} - \mathbf{x}$ or $\mathbf{y} \rightarrow \mathbf{z} = \mathbf{x} - \mathbf{y}$,

$$\int_{\mathbb{R}^d} \frac{u(\mathbf{x}) - u(\mathbf{y})}{|\mathbf{x} - \mathbf{y}|^{d+2s}} d\mathbf{y} = \int_{\mathbb{R}^d} \frac{u(\mathbf{x}) - u(\mathbf{x} + \mathbf{z})}{|\mathbf{z}|^{d+2s}} d\mathbf{z} = \int_{\mathbb{R}^d} \frac{u(\mathbf{x}) - u(\mathbf{x} - \mathbf{z})}{|\mathbf{z}|^{d+2s}} d\mathbf{z}.$$

Therefore, we can alternatively define positive fractional Laplace operators as

$$(-\Delta)^s u(\mathbf{x}) = -\frac{C(d, s)}{2} \int_{\mathbb{R}^d} \frac{u(\mathbf{x} + \mathbf{z}) + u(\mathbf{x} - \mathbf{z}) - 2u(\mathbf{x})}{|\mathbf{z}|^{d+2s}} d\mathbf{z}. \tag{A.4}$$

By Fourier transformation, the above equation implies

$$\begin{aligned} \mathcal{F}[(-\Delta)^s u] &= -\frac{C(d, s)}{2} \int_{\mathbb{R}^d} \frac{\mathcal{F}[u(\mathbf{x} + \mathbf{z}) + u(\mathbf{x} - \mathbf{z}) - 2u(\mathbf{x})]}{|\mathbf{z}|^{d+2s}} d\mathbf{z} \\ &= C(d, s) \left[\int_{\mathbb{R}^d} \frac{1 - \cos \mathbf{k} \cdot \mathbf{z}}{|\mathbf{z}|^{d+2s}} d\mathbf{z} \right] \mathcal{F}[u] \\ &= |\mathbf{k}|^{2s} \mathcal{F}[u]. \end{aligned} \tag{A.5}$$

Similarly, we consider Fourier transformation of (A.1)₂ and obtain

$$\begin{aligned} \mathcal{F}[(-\Delta)^{-s} u] &= \frac{B(d, s)}{2} \int_{\mathbb{R}^d} \frac{\mathcal{F}[u(\mathbf{x} + \mathbf{z}) + u(\mathbf{x} - \mathbf{z})]}{|\mathbf{z}|^{d-2s}} d\mathbf{z} \\ &= B(d, s) \left[\int_{\mathbb{R}^d} \frac{\cos \mathbf{k} \cdot \mathbf{z}}{|\mathbf{z}|^{d-2s}} d\mathbf{z} \right] \mathcal{F}[u] \\ &= |\mathbf{k}|^{-2s} \mathcal{F}[u]. \end{aligned} \tag{A.6}$$

By (A.5) and (A.6), we have

$$\mathcal{F}[(-\Delta)^{-s} (-\Delta)^s u] = |\mathbf{k}|^{-2s} \mathcal{F}[(-\Delta)^s u] = \mathcal{F}[u],$$

which completes the proof of (A.3). For $s_1, s_2 > 0$,

$$(-\Delta)^{-s_1} (-\Delta)^{-s_2} u = (-\Delta)^{-(s_1+s_2)} u,$$

since

$$\mathcal{F}[(-\Delta)^{-s_1} (-\Delta)^{-s_2} u] = |\mathbf{k}|^{-2s_1} \mathcal{F}[(-\Delta)^{-s_2} u] = |\mathbf{k}|^{-2(s_1+s_2)} \mathcal{F}[u]. \tag{A.7}$$

In addition, positive fractional Laplacian $(-\Delta)^{k+s}$ for some positive integer k and $s \in (0, 1)$ can be defined as

$$(-\Delta)^{k+s} u = (-\Delta)^s (-\Delta)^k u = (-\Delta)^k (-\Delta)^s u.$$

Fractional Laplacian operators are self-adjoint and positive definite in the sense that

$$\int_{\mathbb{R}^d} u (-\Delta)^s u = \int_{\mathbb{R}^d} |(-\Delta)^{s/2} u|^2 = \frac{C(d, s)}{2} \int_{\mathbb{R}^d} \int_{\mathbb{R}^d} \frac{|u(\mathbf{x}) - u(\mathbf{y})|^2}{|\mathbf{x} - \mathbf{y}|^{d+2s}} d\mathbf{y} d\mathbf{x}.$$

To see this, by Plancherel's formula we have

$$\begin{aligned} \int_{\mathbb{R}^d} u (-\Delta)^s u d\mathbf{x} &= C(d, s) \int_{\mathbb{R}^d} u(\mathbf{x}) \int_{\mathbb{R}^d} \frac{u(\mathbf{x}) - u(\mathbf{y})}{|\mathbf{x} - \mathbf{y}|^{d+2s}} d\mathbf{y} d\mathbf{x} \\ &= \int_{\mathbb{R}^d} \mathcal{F}[u] \mathcal{F}[(-\Delta)^s u] d\mathbf{k} = \int_{\mathbb{R}^d} |\mathbf{k}|^{2s} |\mathcal{F}[u]|^2 d\mathbf{k} = \int_{\mathbb{R}^d} \left| |\mathbf{k}|^{2s/2} \mathcal{F}[u] \right|^2 d\mathbf{k} \\ &= \int_{\mathbb{R}^d} |(-\Delta)^{s/2} u|^2 d\mathbf{x}, \end{aligned} \tag{A.8}$$

and

$$\begin{aligned} C(d, s) \int_{\mathbb{R}^d} \int_{\mathbb{R}^d} \frac{|u(\mathbf{x}) - u(\mathbf{y})|^2}{|\mathbf{x} - \mathbf{y}|^{d+2s}} d\mathbf{y} d\mathbf{x} &= C(d, s) \int_{\mathbb{R}^d} \int_{\mathbb{R}^d} \frac{1}{|\mathbf{z}|^{d+2s}} (u(\mathbf{z} + \mathbf{x}) - u(\mathbf{x}))^2 d\mathbf{x} d\mathbf{z} \\ &= C(d, s) \int_{\mathbb{R}^d} \frac{1}{|\mathbf{z}|^{d+2s}} \int_{\mathbb{R}^d} (\mathcal{F}[u(\mathbf{z} + \mathbf{x}) - u(\mathbf{x})](\mathbf{k}))^2 d\mathbf{k} d\mathbf{z} \\ &= 2C(d, s) \int_{\mathbb{R}^d} \int_{\mathbb{R}^d} \frac{1 - \cos \mathbf{k} \cdot \mathbf{z}}{|\mathbf{z}|^{d+2s}} (\mathcal{F}[u])^2 d\mathbf{z} d\mathbf{k} \\ &= 2 \int_{\mathbb{R}^d} |\mathbf{k}|^{2s} (\mathcal{F}[u])^2 d\mathbf{k} = 2 \int_{\mathbb{R}^d} |(-\Delta)^{s/2} u|^2 d\mathbf{x}. \end{aligned} \tag{A.9}$$

Appendix B. Scaling of interaction energy and induced field

Let $D \subset \mathbb{R}^d$ be regular bounded domain of lengthscale ~ 1 , $\xi_c \ll 1$ a fixed microscopic lengthscale, and N the number of gridpoints in $D \cap \xi_c \mathbb{Z}^d$. For a smooth compactly supported function $u : \mathbb{R}^d \rightarrow \mathbb{R}$, let

$$S_D[u] = \frac{1}{2} \sum_{i,j=1}^N J(\mathbf{x}_i - \mathbf{x}_j) u(\mathbf{x}_i) u(\mathbf{x}_j) = \frac{v_c}{2} \sum_{i=1}^N u(\mathbf{x}_i) \phi_D(\mathbf{x}_i), \tag{B.1}$$

be a double sum arising from interactions in a discrete model and

$$\phi_D(\mathbf{x}) = \frac{1}{v_c} \sum_{j=1}^N J(\mathbf{x} - \mathbf{x}_j) u(\mathbf{x}_j), \tag{B.2}$$

be the single sum that defines the conjugate of $u(\mathbf{x}_i)$ in the model. Here, the interaction potential is specified in (5.16), i.e., a two-piece function with trivial local interaction and power-law long-range interaction:

$$J(\mathbf{x}) = \begin{cases} J_{\text{core}}(\mathbf{x}) \equiv 0 & \text{if } |\mathbf{x}| < \xi_c, \\ \frac{A_\alpha}{|\mathbf{x}|^\alpha} & \text{if } |\mathbf{x}| \geq \xi_c. \end{cases} \tag{B.3}$$

We are interested in how $S_D[u]$ and $\phi_D(\mathbf{x})$ transform with respect to the following transformation:

$$\begin{aligned} D &\rightarrow D_\lambda = \lambda D = \{\mathbf{y} : \mathbf{y} = \lambda \mathbf{x}, \mathbf{x} \in D\}, \\ u &\rightarrow u_\lambda(\mathbf{y}) = u(\mathbf{y}/\lambda) = u(\mathbf{x}). \end{aligned} \tag{B.4}$$

- Local interaction.** If $\alpha > d+2$, the value of $1/r^\alpha$ decays fast as r increases. First, we focus on the single sum (B.2). If $u : D \rightarrow \mathbb{R}$ is bounded, i.e., $|u| \leq M$ on D for some $M > 0$, the series (B.2) converges absolutely¹⁵ for a fixed ξ_c and as $D \rightarrow \mathbb{R}^d$. In other words, the value of the sum $\phi_D(\mathbf{x})$ is predominantly determined by the ‘‘nearest-neighbor’’ interactions. Let \mathcal{N}_i denote pairs of nearest-neighbors. Then (B.1) and (B.2) may be approximated by

$$\begin{aligned} \phi_D(\mathbf{x}_i) &\approx \frac{1}{v_c} \sum_{\mathbf{x}_j \in \mathcal{N}_i} J(\mathbf{x}_i - \mathbf{x}_j) u(\mathbf{x}_j) \approx \frac{q A_\alpha}{\xi_c^\alpha v_c} u(\mathbf{x}_i), \\ S_D[u] &= \frac{v_c}{2} \sum_{\mathbf{x}_i \in D \cap \xi_c \mathbb{Z}^d} \phi_D(\mathbf{x}_i) u(\mathbf{x}_i) \\ &\rightarrow \frac{1}{2} \int_D \phi_D(\mathbf{x}) u(\mathbf{x}) d\mathbf{x} = \frac{q A_\alpha}{2 \xi_c^\alpha v_c} \int_D u^2(\mathbf{x}) d\mathbf{x}, \end{aligned} \tag{B.5}$$

where q is the number of nearest neighbors for an interior grid point, and the last line follows from the assumption that $u = u(\mathbf{x})$ does not vary significantly over the lengthscale ξ_c . Consequently,

$$\begin{aligned} S_{D_\lambda}[u_\lambda] &\approx \frac{q A_\alpha}{2} \sum_{\mathbf{y}_i \in D_\lambda \cap \xi_c \mathbb{Z}^d} \frac{u_\lambda^2(\mathbf{y}_i)}{\xi_c^\alpha} = \frac{q A_\alpha}{2} \sum_{\mathbf{x}_i \in D \cap \frac{\xi_c}{\lambda} \mathbb{Z}^d} \frac{u^2(\mathbf{x}_i)}{\xi_c^\alpha} \rightarrow \frac{q A_\alpha \lambda^d}{2 \xi_c^\alpha v_c} \int_D u^2(\mathbf{x}) d\mathbf{x} \\ &\approx \lambda^d S_D[u]. \end{aligned} \tag{B.6}$$

- Nonlocal interaction.** If $\alpha = d + 2s \in (d, d + 2)$ for some $s \in (0, 1)$, another approximation of (B.1) may be achieved by directly applying the Euler–Maclaurin’s formula:

$$\begin{aligned} S_D[u] &= \frac{A_\alpha}{2} \sum_{\mathbf{x}_i \in D \cap \xi_c \mathbb{Z}^d} \sum_{\mathbf{x}_j \in D \cap \xi_c \mathbb{Z}^d} \frac{u(\mathbf{x}_i) u(\mathbf{x}_j)}{|\mathbf{x}_i - \mathbf{x}_j|^\alpha} \\ &\rightarrow \frac{A_\alpha}{2 v_c^2} \int_D \int_{(D-\mathbf{x}) \setminus B_{\xi_c}} \frac{u(\mathbf{x}) u(\mathbf{x} + \mathbf{z})}{|\mathbf{z}|^\alpha} d\mathbf{z} d\mathbf{x} \\ &\rightarrow \frac{1}{2 v_c^2} \int_{\mathbb{R}^d} \int_{\mathbb{R}^d} u(\mathbf{x}) u(\mathbf{x} + \mathbf{z}) J(\mathbf{z}) d\mathbf{z} d\mathbf{x}. \end{aligned} \tag{B.7}$$

¹⁵ Convergence of the single sum (B.2) requires only $\alpha > d$.

For the transformed sum, we have

$$\begin{aligned}
 S_{D_\lambda}[u_\lambda] &= \frac{\Lambda_\alpha}{2} \sum_{\mathbf{y}_i \in D_\lambda \cap \xi_c \mathbb{Z}^d} \sum_{\mathbf{y}_j \in D_\lambda \cap \xi_c \mathbb{Z}^d} \frac{u_\lambda(\mathbf{y}_i) u_\lambda(\mathbf{y}_j)}{|\mathbf{y}_i - \mathbf{y}_j|^\alpha} \\
 &= \frac{\Lambda_\alpha}{2} \sum_{\mathbf{x}_i \in D \cap \frac{\xi_c}{\lambda} \mathbb{Z}^d} \sum_{\mathbf{x}_j \in D \cap \frac{\xi_c}{\lambda} \mathbb{Z}^d} \frac{u(\mathbf{x}_i) u(\mathbf{x}_j)}{\lambda^\alpha |\mathbf{x}_i - \mathbf{x}_j|^\alpha} \\
 &\rightarrow \frac{\lambda^{2d-\alpha}}{2v_c^2} \int_{\mathbb{R}^d} \int_{\mathbb{R}^d} u(\mathbf{x}) u(\mathbf{x} + \mathbf{z}) J(\mathbf{z}) d\mathbf{z} d\mathbf{x} \\
 &\approx \lambda^{d-2s} S_D[u],
 \end{aligned} \tag{B.8}$$

where in the last equation we have used that the core interaction potential $J_{\text{core}} \equiv 0$. Meanwhile, from the definition we have

$$\begin{aligned}
 S_D[u] &= \frac{v_c}{2} \sum_{\mathbf{x}_i \in D \cap \xi_c \mathbb{Z}^d} \phi_D(\mathbf{x}_i) u(\mathbf{x}_i) \rightarrow \frac{1}{2} \int_D \phi_D(\mathbf{x}) u(\mathbf{x}) d\mathbf{x}, \\
 S_{D_\lambda}[u_\lambda] &= \frac{v_c}{2} \sum_{\mathbf{y}_i \in D_\lambda \cap \xi_c \mathbb{Z}^d} \phi_{D_\lambda}(\mathbf{y}_i) u_\lambda(\mathbf{y}_i) = \frac{v_c}{2} \sum_{\mathbf{x}_i \in D \cap \frac{\xi_c}{\lambda} \mathbb{Z}^d} \phi_{D_\lambda}(\lambda \mathbf{x}_i) u(\mathbf{x}_i), \\
 &\rightarrow \frac{\lambda^d}{2} \int_D \phi_{D_\lambda}(\lambda \mathbf{x}) u(\mathbf{x}) d\mathbf{x}.
 \end{aligned} \tag{B.9}$$

Comparing (B.8) and (B.9), for consistency we find that the conjugate should transform as

$$\phi_D(\mathbf{x}) \rightarrow \phi_{D_\lambda}(\mathbf{y}) = \lambda^{-2s} \phi_D(\mathbf{y}/\lambda) = \lambda^{-2s} \phi_D(\mathbf{x}). \tag{B.10}$$

3. Long-range interaction. If $\alpha = d - 2s \in (d - 2, d)$ for some $s \in (0, 1)$, the double sum (B.1) diverges if $D \rightarrow \mathbb{R}^d$ (i.e., $\text{size}(D)/\xi_c \rightarrow +\infty$) for a general function $u : \mathbb{R}^d \rightarrow \mathbb{R}$. To have a meaningful result, we assume the state function $u(\mathbf{x})$ decays fast enough such that the conjugate $\phi_D(\mathbf{x})$ is well-defined and can be approximated by a negative fractional Laplace operator (Cf. (A.1)₂)

$$\phi_D(\mathbf{x}) = \frac{1}{v_c} \sum_{j=1}^N \frac{\Lambda_\alpha u(\mathbf{x}_j)}{|\mathbf{x} - \mathbf{x}_j|^{d-2s}} \rightarrow \frac{\Lambda_\alpha}{v_c^2} \int_{\mathbb{R}^d} \frac{u(\mathbf{y})}{|\mathbf{x} - \mathbf{y}|^{d-2s}} d\mathbf{y} = \frac{\Lambda_\alpha}{v_c^2 B(d, s)} (-\Delta)^{-s} u(\mathbf{x}). \tag{B.11}$$

Therefore, the double sum (B.1) may be approximated by:

$$S_D[u] = \frac{\Lambda_\alpha}{v_c^2 B(d, s)} \int_{\mathbb{R}^d} u(\mathbf{x}) (-\Delta)^{-s} u(\mathbf{x}) d\mathbf{x}. \tag{B.12}$$

Under the transformation (B.4), we have

$$\begin{aligned}
 S_D[u] &\rightarrow S_{D_\lambda}[u_\lambda] = \lambda^{d+2s} S_D[u], \\
 \phi_D(\mathbf{x}) &\rightarrow \phi_{D_\lambda}(\mathbf{y}) = \lambda^{2s} \phi_D(\mathbf{y}/\lambda) = \lambda^{2s} \phi_D(\mathbf{x}).
 \end{aligned} \tag{B.13}$$

Appendix C. Strain hardening/softening effects

To account for strain hardening effects, we may consider the activation energy of form (2.3) with $c_1 > 0$. Upon repeating the calculations in Section 4, we have

$$\begin{aligned}
 F &= F^{\text{el}} + F^{\text{pl}}, \\
 F^{\text{el}}(\beta, N, \bar{\sigma}) &= -\frac{V \bar{\sigma}^2}{2G} - \frac{N}{2} k_B T \log T + \text{const}, \\
 F^{\text{pl}} &= -k_B T N \log(Z_1^{\text{pl}})_h,
 \end{aligned} \tag{C.1}$$

where the partition function associated with plastic strain for strain hardening or softening case, $(Z_1^{\text{pl}})_h$, is given by

$$\begin{aligned}
 (Z_1^{\text{pl}})_h &= \sum_{j \in \mathbb{Z}} e^{-v_c \beta \epsilon_a^{\text{pl}} (|j| \sigma_Y + c_1 j^2 \sigma_Y - j \bar{\sigma})} \\
 &= 1 + \sum_{j=1}^{\infty} e^{-(j+c_1 j^2 - j \hat{\sigma})/\hat{T}} + \sum_{j=1}^{\infty} e^{-(j+c_1 j^2 + j \hat{\sigma})/\hat{T}}.
 \end{aligned} \tag{C.2}$$

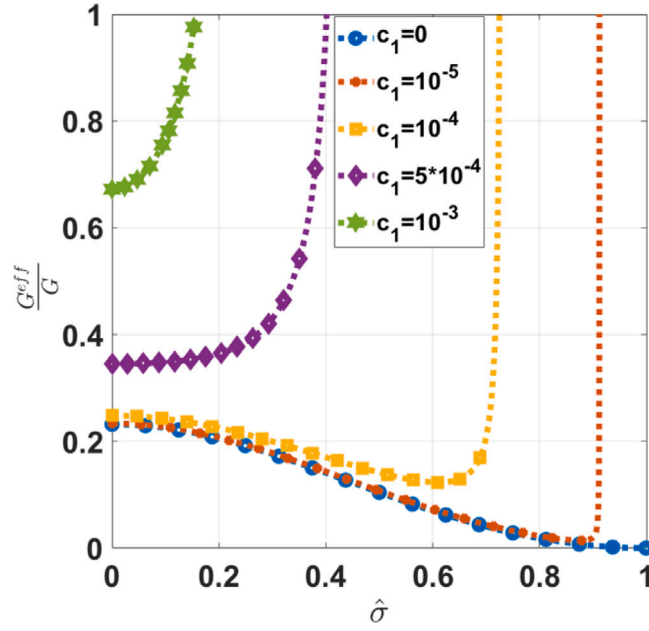


Fig. 7. Plot of $\frac{G^{eff}}{G}$ vs $\hat{\sigma}$ for different c_1 values and at a fixed temperature $T = 300$ K. The independent parameters for the non-interaction model are considered as $\xi_c = 2$ nm, $\sigma_Y = 79$ MPa, $e_c^* = 10^{-4}$, $G = 26$ GPa and $b = 0.286$ nm.

For simplicity, suppose $c_1 \ll 1$.¹⁶ Then the terms on the right-hand side of (C.2) may be approximated as¹⁷

$$\begin{aligned} \sum_{j=1}^{\infty} e^{-(j+c_1j^2-j\hat{\sigma})/\hat{T}} &\approx \sum_{j=1}^{\infty} e^{-j(1-\hat{\sigma})/\hat{T}} - \frac{c_1}{\hat{T}} \sum_{j=1}^{\infty} j^2 e^{-j(1-\hat{\sigma})/\hat{T}} \\ &= \frac{1}{e^{(1-\hat{\sigma})/\hat{T}} - 1} - \frac{c_1}{\hat{T}} \frac{e^{2(1-\hat{\sigma})/\hat{T}} + e^{(1-\hat{\sigma})/\hat{T}}}{(e^{(1-\hat{\sigma})/\hat{T}} - 1)^3}, \\ \sum_{j=1}^{\infty} e^{-(j+c_1j^2+j\hat{\sigma})/\hat{T}} &\approx \sum_{j=1}^{\infty} e^{-j(1+\hat{\sigma})/\hat{T}} - \frac{c_1}{\hat{T}} \sum_{j=1}^{\infty} j^2 e^{-j(1+\hat{\sigma})/\hat{T}} \\ &= \frac{1}{e^{(1+\hat{\sigma})/\hat{T}} - 1} - \frac{c_1}{\hat{T}} \frac{e^{2(1+\hat{\sigma})/\hat{T}} + e^{(1+\hat{\sigma})/\hat{T}}}{(e^{(1+\hat{\sigma})/\hat{T}} - 1)^3}, \end{aligned} \quad (C.3)$$

and, F^{pl} simplifies as,

$$\begin{aligned} F^{pl} &= F_0^{pl} + F_1^{pl}, \\ F_0^{pl} &= -k_B T N \log(Z_1^p), \quad Z_1^p = 1 + \frac{1}{e^{(1-\hat{\sigma})/\hat{T}} - 1} + \frac{1}{e^{(1+\hat{\sigma})/\hat{T}} - 1}, \\ F_1^{pl} &:= N \frac{c_1 v_c e_c^p \sigma_Y}{Z_1^p} \left[\frac{e^{2(1-\hat{\sigma})/\hat{T}} + e^{(1-\hat{\sigma})/\hat{T}}}{(e^{(1-\hat{\sigma})/\hat{T}} - 1)^3} + \frac{e^{2(1+\hat{\sigma})/\hat{T}} + e^{(1+\hat{\sigma})/\hat{T}}}{(e^{(1+\hat{\sigma})/\hat{T}} - 1)^3} \right]. \end{aligned} \quad (C.4)$$

Substituting (C.4) in (C.1), we obtain the total free energy F . Using this total free energy F and (3.9), we evaluate the effective macroscopic shear modulus G^{eff} . Fig. 7 shows plot of $\frac{G^{eff}}{G}$ vs $\hat{\sigma}$ for different c_1 values and at a fixed temperature $T = 300$ K. We observe that, for a fixed applied stress $\hat{\sigma}$, the effective macroscopic shear modulus (G^{eff}) increases with an increase in c_1 value, indicating the strain hardening effect.

References

- Abkevich, V.I., Gutin, A.M., Shakhnovich, E.I., 1995. Impact of local and non-local interactions on thermodynamics and kinetics of protein folding. *J. Mol. Biol.* 252 (4), 460–471.
- Ahmadpoor, Fatemeh, Wang, Peng, Huang, Rui, Sharma, Pradeep, 2017. Thermal fluctuations and effective bending stiffness of elastic thin sheets and graphene: A nonlinear analysis. *J. Mech. Phys. Solids* 107, 294–319.

¹⁶ In hindsight, the subsequent approximations are reasonable as long as the right hand sides of (C.3) make sense.

¹⁷ The infinite series $\sum_{j=1}^{\infty} j^2 e^{-jx} = 1 \sum_{j=1}^{\infty} e^{-jx} j'' = \frac{x^2(1+e^{-x})}{(e^{-x}-1)^3}$.

- Ahmadpoor, Fatemeh, Zou, Guijin, Gao, Huajian, 2022. Entropic interactions of 2D materials with cellular membranes: Parallel versus perpendicular approaching modes. *Mech. Mater.* 174, 104414.
- Al-Rub, Rashid K. Abu, Voyiadjis, George Z., 2006. A physically based gradient plasticity theory. *Int. J. Plast.* 22 (4), 654–684.
- Alizadeh, A., Sharma, P., Ganti, S., LeBoeuf, S.F., Tsakalakos, L., 2004. Templated wide band-gap nanostructures. *J. Appl. Phys.* 95 (12), 8199–8206.
- Ashby, M.F., 1970. The deformation of plastically non-homogeneous materials. *Philos. Mag.: J. Theoret. Exp. Appl. Phys.* 21 (170), 399–424.
- Berdichevsky, V.L., 2023. On temperature scaling in dislocation plasticity. *J. Mech. Phys. Solids* 170, 105102.
- Bologna, E., Di Paola, M., Dayal, K., Deseri, Luca, Zingales, M., 2020. Fractional-order nonlinear hereditarity of tendons and ligaments of the human knee. *Phil. Trans. R. Soc. A* 378 (2172), 20190294.
- Bruus, Henrik, Flensberg, Karsten, 2004. *Many-Body Quantum Theory in Condensed Matter Physics: An Introduction*. OUP Oxford.
- Bushby, A.J., Dunstan, D.J., 2004. Plasticity size effects in nanoindentation. *J. Mater. Res.* 19 (1), 137–142.
- Campa, Alessandro, Dauxois, Thierry, Ruffo, Stefano, 2009. Statistical mechanics and dynamics of solvable models with long-range interactions. *Phys. Rep.* 480 (3–6), 57–159.
- Carreker, R.P., Hibbard, W.R., 1957. Tensile deformation of aluminum as a function of temperature, strain rate, and grain size. *JOM* 9, 1157–1163.
- Chen, Dengke, Kulkarni, Yashashree, 2013. Elucidating the kinetics of twin boundaries from thermal fluctuations. *MRS Commun.* 3 (4), 241–244.
- Chen, Dengke, Kulkarni, Yashashree, 2015. Entropic interaction between fluctuating twin boundaries. *J. Mech. Phys. Solids* 84, 59–71.
- Chen, Dengke, Kulkarni, Yashashree, 2017. Thermal fluctuations as a computational microscope for studying crystalline interfaces: A mechanistic perspective. *J. Appl. Mech.* 84 (12), 121001.
- Dahlberg, Carl F.O., Boåsen, Magnus, 2019. Evolution of the length scale in strain gradient plasticity. *Int. J. Plast.* 112, 220–241.
- Dahlberg, Carl F.O., Faleskog, Jonas, 2013. An improved strain gradient plasticity formulation with energetic interfaces: theory and a fully implicit finite element formulation. *Comput. Mech.* 51, 641–659.
- Dahlberg, Carl F.O., Faleskog, Jonas, 2014. Strain gradient plasticity analysis of the influence of grain size and distribution on the yield strength in polycrystals. *Eur. J. Mech. A Solids* 44, 1–16.
- Dahlberg, Carl F.O., Ortiz, Michael, 2019. Fractional strain-gradient plasticity. *Eur. J. Mech. A Solids* 75, 348–354.
- Deseri, Luca, Pollaci, Pietro, Zingales, M., Dayal, K., 2016. Fractional hereditarity of lipid membranes: Instabilities and linearized evolution. *J. Mech. Behav. Biomed. Mater.* 58, 11–27.
- Di Nezza, Eleonora, Palatucci, Giampiero, Valdinoci, Enrico, 2012. Hitchhiker's guide to the fractional Sobolev spaces. *Bull. Sci. Mathématiques* 136 (5), 521–573.
- Di Paola, Mario, Zingales, Massimiliano, 2008. Long-range cohesive interactions of non-local continuum faced by fractional calculus. *Int. J. Solids Struct.* 45 (21), 5642–5659.
- Dimiduk, Dennis M., Koslowski, Marisol, LeSar, Richard, 2006. Preface to the viewpoint set on: Statistical mechanics and coarse graining of dislocation behavior for continuum plasticity. *Scr. Mater.* 54 (5), 701–704.
- Ding, Wei, Patnaik, Sansit, Sidhardh, Sai, Semperlotti, Fabio, 2021. Applications of distributed-order fractional operators: A review. *Entropy* 23 (1), 110.
- Dunstan, D.J., Ehrler, B., Bossis, R., Joly, S., P'ng, K.M.Y., Bushby, A.J., 2009. Elastic limit and strain hardening of thin wires in torsion. *Phys. Rev. Lett.* 103 (15), 155501.
- El-Azab, Anter, 2000. Statistical mechanics treatment of the evolution of dislocation distributions in single crystals. *Phys. Rev. B* 61 (18), 11956.
- Eringen, A. Cemal, 1972. Linear theory of nonlocal elasticity and dispersion of plane waves. *Internat. J. Engrg. Sci.* 10 (5), 425–435.
- Evans, Anthony G., Hutchinson, John W., 2009. A critical assessment of theories of strain gradient plasticity. *Acta Mater.* 57 (5), 1675–1688.
- Fleck, N.A., Hutchinson, J.W., 2001. A reformulation of strain gradient plasticity. *J. Mech. Phys. Solids* 49 (10), 2245–2271.
- Fleck, N.A., Hutchinson, J.W., Willis, J.R., 2015. Guidelines for constructing strain gradient plasticity theories. *J. Appl. Mech.* 82 (7), 071002.
- Fleck, N.A., Muller, G.M., Ashby, Mike F., Hutchinson, John W., 1994. Strain gradient plasticity: theory and experiment. *Acta Metall. Mater.* 42 (2), 475–487.
- Fleck, N.A., Willis, J.R., 2009a. A mathematical basis for strain-gradient plasticity theory—Part I: Scalar plastic multiplier. *J. Mech. Phys. Solids* 57 (1), 161–177.
- Fleck, N.A., Willis, J.R., 2009b. A mathematical basis for strain-gradient plasticity theory. Part II: Tensorial plastic multiplier. *J. Mech. Phys. Solids* 57 (7), 1045–1057.
- Fredriksson, Per, Gudmundson, Peter, 2005. Size-dependent yield strength of thin films. *Int. J. Plast.* 21 (9), 1834–1854.
- French, Roger H., Parsegian, V. Adrian, Podgornik, Rudolf, Rajter, Rick F., Jagota, Anand, Luo, Jian, Asthagiri, Dilip, Chaudhury, Manoj K., Chiang, Yet-ming, Granick, Steve, et al., 2010. Long range interactions in nanoscale science. *Rev. Modern Phys.* 82 (2), 1887.
- Gao, Huajian, Huang, Yonggang, 2003. Geometrically necessary dislocation and size-dependent plasticity. *Scr. Mater.* 48 (2), 113–118.
- Grasinger, Matthew, Majidi, Carmel, Dayal, Kaushik, 2021. Nonlinear statistical mechanics drives intrinsic electrostriction and volumetric torque in polymer networks. *Phys. Rev. E* 103 (4), 042504.
- Grasinger, Matthew, Sharma, Pradeep, 2024. Thermal fluctuations (eventually) unfold nanoscale origami. *J. Mech. Phys. Solids* 184, 105527.
- Greer, Julia R., De Hosson, Jeff Th M., 2011. Plasticity in small-sized metallic systems: Intrinsic versus extrinsic size effect. *Prog. Mater. Sci.* 56 (6), 654–724.
- Gudmundson, Peter, 2004. A unified treatment of strain gradient plasticity. *J. Mech. Phys. Solids* 52 (6), 1379–1406.
- Gurtin, Morton E., Anand, Lallit, 2009. Thermodynamics applied to gradient theories involving the accumulated plastic strain: the theories of aifantis and fleck and hutchinson and their generalization. *J. Mech. Phys. Solids* 57 (3), 405–421.
- Han, Chung-Souk, Gao, Huajian, Huang, Yonggang, Nix, William D., 2005. Mechanism-based strain gradient crystal plasticity—I. Theory. *J. Mech. Phys. Solids* 53 (5), 1188–1203.
- Hill, Rodney, 1998. *The Mathematical Theory of Plasticity*. vol. 11, Oxford University Press.
- Hollkamp, John P., Semperlotti, Fabio, 2020. Application of fractional order operators to the simulation of ducts with acoustic black hole terminations. *J. Sound Vib.* 465, 115035.
- Huang, Shenglin, Graham, Ian R., Riggleman, Robert A., Arratia, Paulo E., Fitzgerald, Steve, Reina, Celia, 2022. Predicting the unobserved: A statistical mechanics framework for non-equilibrium material response with quantified uncertainty. *J. Mech. Phys. Solids* 161, 104779.
- Hutchinson, John, Fleck, Norman, 1997. Strain gradient plasticity. *Adv. Appl. Mech.* 33, 295–361.
- Idiart, M.I., Deshpande, V.S., Fleck, N.A., Willis, J.R., 2009. Size effects in the bending of thin foils. *Internat. J. Engrg. Sci.* 47 (11–12), 1251–1264.
- Idiart, Martín I., Fleck, Norman A., 2009a. Size effects in the torsion of thin metal wires. *Modelling Simul. Mater. Sci. Eng.* 18 (1), 015009.
- Idiart, Martín I., Fleck, Norman A., 2009b. Size effects in the torsion of thin metal wires. *Modelling Simul. Mater. Sci. Eng.* 18 (1), 015009.
- Jha, Prashant K., Breitzman, Timothy, Dayal, Kaushik, 2023. Discrete-to-continuum limits of long-range electrical interactions in nanostructures. *Arch. Ration. Mech. Anal.* 247 (2), 29.
- Khandagale, Pratik, Breitzman, Timothy, Majidi, Carmel, Dayal, Kaushik, 2023. Statistical field theory for nonlinear elasticity of polymer networks with excluded volume interactions. *Phys. Rev. E* 107 (6), 064501.
- Khandagale, Pratik, Garcia-Cervera, Carlos, Debotton, Gal, Breitzman, Timothy, Majidi, Carmel, Dayal, Kaushik, 2024. Statistical field theory of polarizable polymer chains with nonlocal dipolar interactions. *Phys. Rev. E* 109 (4), 044501.
- Korte, S., Clegg, W.J., 2011. Discussion of the dependence of the effect of size on the yield stress in hard materials studied by microcompression of MgO. *Phil. Mag.* 91 (7–9), 1150–1162.
- Kröner, E., 1967. Elasticity theory of materials with long range cohesive forces. *Int. J. Solids Struct.* 3 (5), 731–742.
- Kulkarni, Yashashree, 2023. Fluctuations of active membranes with nonlinear curvature elasticity. *J. Mech. Phys. Solids* 173, 105240.

- Kuroda, Mitsutoshi, Needleman, Alan, 2019. A simple model for size effects in constrained shear. *Extreme Mech. Lett.* 33, 100581.
- Lazopoulos, KA22457841192, 2006. Non-local continuum mechanics and fractional calculus. *Mech. Res. Commun.* 33 (6), 753–757.
- Leadbetter, Travis, Purohit, Prashant K., Reina, Celia, 2023. A statistical mechanics framework for constructing nonequilibrium thermodynamic models. *PNAS Nexus* 2 (12), p. 417.
- Li, Jun, Ostoja-Starzewski, Martin, 2009. Fractal solids, product measures and fractional wave equations. *Proc. R. Soc. A: Math. Phys. Eng. Sci.* 465 (2108), 2521–2536.
- Li, Jun, Ostoja-Starzewski, Martin, Tarasov, Vasily E., 2019. Application of fractional calculus to fractal media. *Appl. Phys. A* 263–276.
- Limkumnerd, Surachate, Van der Giessen, Erik, 2008. Statistical approach to dislocation dynamics: From dislocation correlations to a multiple-slip continuum theory of plasticity. *Phys. Rev. B* 77 (18), 184111.
- Liu, Dabiao, He, Yuming, Dunstan, David J., Zhang, Bo, Gan, Zhipeng, Hu, Peng, Ding, Huaming, 2013. Toward a further understanding of size effects in the torsion of thin metal wires: an experimental and theoretical assessment. *Int. J. Plast.* 41, 30–52.
- Liu, L.P., Sharma, P., 2013. Flexoelectricity and thermal fluctuations of lipid bilayer membranes: Renormalization of flexoelectric, dielectric, and elastic properties. *Phys. Rev. E* 87 (3), 032715.
- Marshall, Jason, Dayal, Kaushik, 2014. Atomistic-to-continuum multiscale modeling with long-range electrostatic interactions in ionic solids. *J. Mech. Phys. Solids* 62, 137–162.
- Mashayekhi, Somayeh, Hussaini, M. Yousuff, Oates, William, 2019. A physical interpretation of fractional viscoelasticity based on the fractal structure of media: Theory and experimental validation. *J. Mech. Phys. Solids* 128, 137–150.
- Mashayekhi, Somayeh, Miles, Paul, Hussaini, M. Yousuff, Oates, William S., 2018. Fractional viscoelasticity in fractal and non-fractal media: Theory, experimental validation, and uncertainty analysis. *J. Mech. Phys. Solids* 111, 134–156.
- Mu, Yang, Hutchinson, J.W., Meng, W.J., 2014. Micro-pillar measurements of plasticity in confined Cu thin films. *Extreme Mech. Lett.* 1, 62–69.
- Mu, Yang, Zhang, Xiaoman, Hutchinson, J.W., Meng, W.J., 2016. Dependence of confined plastic flow of polycrystalline Cu thin films on microstructure. *MRS Commun.* 6 (3), 289–294.
- Mühlhaus, H.-B., Alfantis, EC1122718, 1991. A variational principle for gradient plasticity. *Int. J. Solids Struct.* 28 (7), 845–857.
- Neumann, J.v., 1928. Zur theorie der gesellschaftsspiele. *Math. Ann.* 100 (1), 295–320.
- Niordson, Christian F., Hutchinson, John W., 2011. Basic strain gradient plasticity theories with application to constrained film deformation. *J. Mech. Mater. Struct.* 6 (1), 395–416.
- Niordson, Christian F., Legarth, Brian Nyvang, 2010. Strain gradient effects on cyclic plasticity. *J. Mech. Phys. Solids* 58 (4), 542–557.
- Nye, John F., 1953. Some geometrical relations in dislocated crystals. *Acta Metall.* 1 (2), 153–162.
- Oates, William, Stanisaukis, Eugenia, Pahari, Basanta R., Mashayekhi, Somayeh, 2021. Entropy dynamics approach to fractional order mechanics with applications to elastomers. In: *Behavior and Mechanics of Multifunctional Materials XV*. Vol. 11589, SPIE, pp. 23–34.
- Ostojca-Starzewski, Martin, 2009. Continuum mechanics models of fractal porous media: Integral relations and extremum principles. *J. Mech. Mater. Struct.* 4 (5), 901–912.
- Ostojca-Starzewski, Martin, 2013. Electromagnetism on anisotropic fractal media. *Z. Angew. Math. Phys.* 64, 381–390.
- Patnaik, Sansit, Hollkamp, John P., Semperlotti, Fabio, 2020a. Applications of variable-order fractional operators: a review. *Proc. R. Soc. A* 476 (2234), 20190498.
- Patnaik, Sansit, Sidhardh, Sai, Semperlotti, Fabio, 2020b. Geometrically nonlinear analysis of nonlocal plates using fractional calculus. *Int. J. Mech. Sci.* 179, 105710.
- Rohrer, Gregory S., Chesser, Ian, Krause, Amanda R., Naghibzadeh, S. Kiana, Xu, Zipeng, Dayal, Kaushik, Holm, Elizabeth A., 2023. Grain boundary migration in polycrystals. *Annu. Rev. Mater. Res.* 53.
- Sethna, James P., Bierbaum, Matthew K., Dahmen, Karin A., Goodrich, Carl P., Greer, Julia R., Hayden, Lorien X., Kent-Dobias, Jaron P., Lee, Edward D., Liarte, Danilo B., Ni, Xiaoyue, et al., 2017. Deformation of crystals: Connections with statistical physics. *Annu. Rev. Mater. Res.* 47, 217–246.
- Soutyryne, V.G., Berdichevsky, V.L., 2018. Statistical properties of edge dislocation ensembles. *Phil. Mag.* 98 (33), 2982–3006.
- Voyiadjis, George Z., Song, Yooseob, 2019. Strain gradient continuum plasticity theories: theoretical, numerical and experimental investigations. *Int. J. Plast.* 121, 21–75.
- Xiang, Yang, Vlassak, Joost J., 2006. Bauschinger and size effects in thin-film plasticity. *Acta Mater.* 54 (20), 5449–5460.
- Yefimov, S., Van der Giessen, E., 2005. Multiple slip in a strain-gradient plasticity model motivated by a statistical-mechanics description of dislocations. *Int. J. Solids Struct.* 42 (11–12), 3375–3394.
- Yefimov, S., Groma, István, Van der Giessen, E., 2004. A comparison of a statistical-mechanics based plasticity model with discrete dislocation plasticity calculations. *J. Mech. Phys. Solids* 52 (2), 279–300.
- Yukawa, Hideki, 1950. Quantum theory of non-local fields. Part I. Free fields. *Phys. Rev.* 77 (2), 219.
- Zhu, Fangyan, Leng, Jiantao, Jiang, Jin-Wu, Chang, Tienchong, Zhang, Tongyi, Gao, Huajian, 2022. Thermal-fluctuation gradient induced tangential entropic forces in layered two-dimensional materials. *J. Mech. Phys. Solids* 163, 104871.